Atmos. Chem. Phys. Discuss., 9, 16381–16439, 2009
www.atmos-chem-phys-discuss.net/9/16381/2009/

Atmospheric Chemistry and Physics Discussions

This discussion paper is/has been under review for the journal *Atmospheric Chemistry and Physics (ACP)*. Please refer to the corresponding final paper in *ACP* if available.

Trans-Pacific transport and evolution of aerosols and trace gases from Asia during the INTEX-B field campaign

B. Adhikary[1,*], G. R. Carmichael[1], S. Kulkarni[1], C. Wei[1], Y. Tang[1,], A. Dallura[1,***], M. Mena-Carrasco[1,****], D. G. Streets[2], Q. Zhang[2], R. B. Pierce[3,*****], J. A. Al-Saadi[3], L. K. Emmons[4], G. G. Pfister[4], M. A. Avery[3], J. D. Barrick[3], D. R. Blake[5], W. H. Brune[6], R. C. Cohen[7], J. E. Dibb[8], A. Fried[4], B. G. Heikes[9], L. G. Huey[10], D. W. O'Sullivan[11], G. W. Sachse[3], R. E. Shetter[4], H. B. Singh[12], T. L. Campos[4], C. A. Cantrell[4], F. M. Flocke[4], E. J. Dunlea[13,******], J. L. Jimenez[13], A. J. Weinheimer[4], J. D. Crounse[14], P. O. Wennberg[14], J. J. Schauer[15], E. A. Stone[15], D. A. Jaffe[16], and D. R. Reidmiller[17]**

[1]Center for Global and Regional Environmental Research, University of Iowa, Iowa City, IA 52242, USA

[2] Decision and Information Sciences Division, Argonne National Laboratory, Argonne, IL, USA
[3] NASA Langley Research Center, Hampton, VA, USA
[4] National Center for Atmospheric Research, Boulder, CO, USA
[5] Department of Chemistry, University of California, Irvine, CA, USA
[6] Department of Meteorology, Penn State University, University Park, PA, USA
[7] Department of Chemistry, University of California, Berkeley, CA, USA
[8] Institute for the Study of Earth, Oceans and Space, University of New Hampshire, Durham, NH, USA
[9] Graduate School of Oceanography, University of Rhode Island, Narragansett, RI, USA
[10] School of Earth and Atmospheric Sciences, Georgia Institute of Technology, Atlanta, GA, USA
[11] United States Naval Academy, Annapolis, MD, USA
[12] NASA Ames Research Center, Moffett Field, CA, USA
[13] Department of Chemistry and Biochemistry, and CIRES, University of Colorado, Boulder, CO, USA
[14] California Institute of Technology, Pasadena, CA, USA
[15] Environmental Chemistry and Technology, College of Engineering, University of Wisconsin-Madison, Madison, WI, USA
[16] University of Washington, Bothell, WA 98011, USA
[17] Department of Atmospheric Sciences/University of Washington, Seattle, WA 98195, USA
[*] now at: School of Engineering, Kathmandu University, P.O. Box 6250, Dhulikhel, Nepal
[**] now at: NOAA/NCEP/EMC, Camp Springs, MD, USA
[***] now at: ARIANET Srl, Via Gilino, 20128, Milano, Italy
[****] now at: Universidad Andrés Bello, Department of Environmental Engineering, Santiago, Chile
[*****] now at: Advanced Satellite Products Branch, NOAA/NESDIS/STAR/CIMSS, Madison, WI, USA

ACPD
9, 16381–16439, 2009

****** now at: NOAA Climate Program Office, Silver Spring, MD, USA

Received: 19 July 2009 – Accepted: 24 July 2009 – Published: 3 August 2009

Correspondence to: S. Kulkarni (sarika-kulkarni@uiowa.edu)

Published by Copernicus Publications on behalf of the European Geosciences Union.

Abstract

The Sulfur Transport and dEposition Model (STEM) developed at the University of Iowa is applied to the analysis of observations obtained during the Intercontinental Chemical Transport Experiment-Phase B (INTEX-B), conducted over the Pacific Ocean during the 2006 North American spring season. This paper reports on the model performance of meteorological parameters, trace gases, aerosols and photolysis rate (J-values) predictions with the NASA DC-8 and NSF/NCAR C-130 airborne measurements along with observations from three surface sites Mt. Bachelor, Trinidad Head and Kathmandu, Nepal. In general the model shows appreciable skill in predicting many of the important aspects of the observed distributions. The major meteorological parameters driving long range transport are accurately predicted by the WRF simulations used in this study. Furthermore, the STEM model predicts aerosols and trace gases concentrations within a standard deviation of most of the observed mean values. The results also point towards areas where model improvements are needed; e.g., the STEM model underestimates CO (15% for the DC8 and 6% for the C-130), whereas it overpredicts PAN (by a factor of two for both aircraft). The errors in the model calculations are attributed to uncertainty in emissions estimates and uncertainty in the top and lateral boundary conditions. Results from a series of sensitivity simulations examining the impact of the growth of emissions in Asia from 2000 to 2006, the importance of biomass burning, the effect of using boundary conditions from different global models, and the role of heterogeneous chemistry on the predictions are also presented. The impacts of heterogeneous reactions at specific times during dust transport episodes can be significant, and in the presence of dust both sulfate and nitrate aerosol production is increased and gas phase nitric acid levels are reduced appreciably (~50%). The aging of the air masses during the long range transport over the Pacific and the impact of various sources (source regions as well as energy and biomass burning) on targeted observations are analyzed using back-trajectories and tagged CO-tracer analysis.

ACPD

9, 16381–16439, 2009

1 Introduction

Economic development in the last few decades throughout much of Asia has led to rapid increase in anthropogenic emissions of aerosols and trace gases (Streets et al., 2003; Garg et al., 2006). Studies have shown that some of these aerosols and trace gases emitted from Asia reach North America and significantly enhance ozone and aerosol concentration over background levels (Jaffe et al., 1999; VanCuren, 2003; Hadley et al., 2007; Van Donkelaar et al., 2008; Zhang et al., 2008). The transport of pollutants from the Asian mid-latitudes to North America is particularly strong during the spring season (Yienger et al., 2000; Bey et al., 2001; Liang et al., 2004). Long range transport of aerosols and gaseous pollutants could partially offset domestic emission controls over North America. In addition, rising Asian aerosol emissions may have a climatic impact on North America (Levy et al., 2008).

The Intercontinental Chemical Transport Experiment, Phase B (INTEX-B) campaign was conducted during the spring of 2006 by the National Aeronautics and Space Administration (NASA) (Singh et al., 2009). One of the scientific objectives of the INTEX-B field campaign was to understand the transport and evolution of Asian pollution with implications for North American air quality and climate. Multiple airborne measurements from the NASA-DC-8 and the NSF/NCAR C-130 aircraft were made to characterize the atmospheric environment of the Pacific and Western North America (Dunlea et al., 2008; McNaughton et al., 2009; Shinozuka et al., 2009; Singh et al., 2009). In addition to the airborne measurements, observations from different remote sensing instruments on board the NASA satellites and various ground based surface stations were also made (e.g. Wolfe et al., 2007; Reidmiller et al., 2009). Global and regional chemical transport models were used to assist the flight planning of the airborne observation missions.

The Sulfur Transport and dEposition Model (STEM) is a regional chemical transport model that was deployed in the flight planning during the INTEX-B field campaign. This model was also used to interpret observations made from the airborne platforms. De-

ACPD
9, 16381–16439, 2009

spite the uncertainties inherent in chemical transport models, they provide valuable means to link observed pollutant concentrations with their emission sources. Chemical transport models are also used to interpret the formation/destruction of chemical species as they are transported away from source regions. One of the major advantages of modeling studies is its ability to provide continuous 3 dimensional distributions of pollutants across a wide geographical space so that effective mitigation strategies can be designed.

Several airborne campaigns in the recent past have been conducted to study the rising impact of Asian pollution over the Pacific and North America. The TRACE-P and ACE-Asia studied the outflow of Asian emissions to the Western Pacific during the spring of 2001 (Jacob et al., 2003; Seinfeld et al., 2004). PHOBEA-II and ITCT-2K2 field campaigns were undertaken to characterize the atmospheric environment of the Eastern Pacific during the spring of 2001 and 2002, respectively (Bertschi et al., 2004). The INTEX-B campaign with the NASA DC-8 aircraft stationed over Hawaii and Anchorage and the NSF/NCAR C-130 stationed over Seattle provided a much better geographical coverage of the inflow of Asian emissions to the East Central Pacific and Western North America.

Tang et al. (2003) evaluated the role of aerosols in influencing photochemistry over the Western Pacific during the TRACE-P mission (Tang et al., 2003). The study found that aerosol influence via photolysis rate (J-values) reduced OH by 40% below 1 km and by 24% above 1 km. The INTEX-B airborne observations constrain the model across a wider geographical region and provide an opportunity to examine the contribution of aerosols in influencing photochemistry farther away from the source region. Aerosols can also influence atmospheric chemistry by providing surface area where reactions can occur (Grassian, 2002). A previous version of the STEM model has also been used to study the impact of heterogeneous chemistry on dust surfaces during the ACE-Asia campaign (Tang et al., 2004b). The results from ACE-Asia study showed that near the surface layer heterogeneous reactions decreased the concentration of O_3, SO_2, NO_2 and HNO_3 by 20%, 55%, 20% and 95%. The INTEX-B observations al-

ACPD
9, 16381–16439, 2009

low us to study the influence of heterogeneous reactions with a longer time for aerosol transport, mixing and ageing for possible implications to atmospheric composition over North America.

In this paper we present an analysis of the INTEX-B observations using our regional scale model. We first present a description of our regional model description and the emissions inventory we used for this study (Sect. 2). We then discuss the transport of trace gases and aerosols across the Pacific (Sect. 3). STEM model predictions are evaluated with data obtained from the INTEX-B DC-8 and C-130 aircraft along with data from two surface sites in Western US and one from Asia during the same time period. We also use the model to identify observed pollutant source regions using back trajectory and region tagged CO tracers. Using the modeled back trajectories we identify several cases of possible quasi lagrangian sampling between the airborne platforms and North American ground based observation sites. We then use the model to assess the impact of rising Asian anthropogenic emissions and the contribution of biomass burning to observations. Finally, we present the model based discussion of pollutant evolution, the impact of heterogeneous chemistry on dust aerosol surfaces and the contribution of aerosols in influencing photochemistry over the Pacific.

2 Model description and emissions inventory

The STEM model was developed at the University of Iowa in the early 1980s (Carmichael et al., 1986) and has continuously undergone development since then to its current version which is the STEM-2K3 version (Tang et al., 2007). The STEM model is a regional chemical transport model which features the SAPRC-99 chemical mechanism (Carter, 2000). Online photolysis rate calculations in the STEM model are performed using the TUV (Tropospheric Ultra-Violet Radiation) model (Madronich, 2002). The TUV model needs total ozone column to calculate the absorption of UV radiation by ozone molecules. Since STEM model is a regional model simulating the troposphere, column ozone data from satellite is used. For this study, we have used

ACPD
9, 16381–16439, 2009

the column ozone data from the Ozone Mapping Spectrometer (OMI) (including STEM calculation for the troposphere) instrument on board the NASA Aura spacecraft. Thirty different photolysis rates are calculated using the STEM-TUV model. The STEM model uses the SCAPE II (Simulating Composition of Atmospheric Particles in Equilibrium Aerosol Solver) aerosol module to simulate inorganic gas to particle conversion and aerosol particle growth (Kim et al., 1995). The inorganic aerosols in the STEM-SCAPE model are binned into four size bins of 0.1–0.3 μm, 0.3–1.0 μm, 1.0–2.5 μm and 2.5–10.0 μm. The model was run for the entire INTEX-B field campaign with 1 week for model spin up.

STEM does not require a uniform horizontal grid and can be mapped to any map projection based on the meteorological model. STEM preprocessor extracts all of the topography and other land use variables that were used in the meteorological model along with the meteorological parameters necessary for simulating chemical transport and removal processes. Thus, STEM has the same map projection and grid resolution as the meteorological model. For this study, we used the WRF-ARW (Weather Research Forecasting) Version 2.1.2 meteorological model developed at NCAR (Skamarock et al., 2005). The WRF model horizontal resolution was 50×50 km with 314×200 grid cells. The model has 21 vertical levels with the model top at 50 hPa. Vertical spacing was defined to have the highest density in the first kilometer. STEM is parameterized to simulate the tropospheric pollutant transport and chemistry. Therefore the chemistry model was simulated with only the first 18 layers reaching up to 10.5 km above ground layer (AGL) height. Significant stratospheric air-mass intrusion within the model domain at higher latitudes (without any stratospheric chemistry/parameterization in the STEM model) limited the chemistry model's ability to simulate higher altitudes. GFS 1°×1° model forecast at 18:00 UTC from the National Center for Environmental Prediction (NCEP) was used to initialize the WRF model and as a boundary condition at every 6 h interval. The physics options used in the WRF model are as follows: WSM-3 class simple ice scheme for microphysics, RRTM scheme for longwave/shortwave radiation, Monin-Obukhov scheme for surface layer, Noah land-surface model, YSU

ACPD
9, 16381–16439, 2009

scheme for the boundary layer option and Grell-Devenyi ensemble scheme for the cumulus parameterization. Evaluation of WRF model prediction skills with INTEX-B observation is presented in the next section.

Gridded anthropogenic emissions for Asia were obtained from the emissions inventory developed for the INTEX-B mission (Zhang et al., 2009). The horizontal resolution of the gridded emissions inventory was 0.5×0.5 degrees ranging from 8–50 degree north latitude and from 80–150 degrees east longitude. Emissions of volatile organic compounds were available based on the SAPRC-99 speciation. For the North American region we used the National Emissions Estimate (NEI-2001v3) from Jeff Vukovich who updated the NEI 1999 emissions from the US Environmental Protection Agency. This emissions inventory has been previously used to study the regional air quality over North America during the ICARTT mission (Mena-Carrasco et al., 2007; Tang et al., 2007). For regions outside the INTEX-B Asia and North America domains we used the global emissions inventory from the EDGAR database (Olivier et al., 2001). To perform a sensitivity study of increasing Asian emissions, we use the TRACE-P emissions inventory which were based on the emissions for the year 2000 (Streets et al., 2003) and compare it with the INTEX-B emissions. Daily emissions forecast from biomass burning were available from the Regional Air Quality Modeling System (RAQMs) modeling group during the INTEX-B field campaign (Al-Saadi et al., 2008). We use the same biomass burning emissions for this post field mission study. Biogenic emissions of terpene and isoprene are taken from a 12 year averaged data from the ORCHIDEE model (Lathiere et al., 2006). It has been shown that using the top and lateral boundary conditions from a global model enhances STEM model prediction skill (Tang et al., 2007). So we have used the Model for Ozone and Related Chemical Tracers (MOZART-4) global model to provide top and lateral boundary conditions (Pfister et al., 2008) for this study. Dust emissions are calculated online using a parameterization based on previous studies using the STEM model (Tang et al., 2004b; Uno et al., 2004). Emissions of sea salt within the STEM model are based on the work by S. L. Gong (Gong, 2003).

ACPD
9, 16381–16439, 2009

3 Results and discussion

3.0.1 Spatial distribution of CO, O_3 and HO_x

Figure 1a shows the horizontal modeling domain of the WRF-STEM model. Figure 1a and b also show the flight tracks of the DC-8 and the C-130 during the INTEX-B field campaign. As shown in Fig. 1, there is substantial amount of geographic space covered by the DC-8 flights over the Central Pacific while the C-130 airborne observations cover a good portion of the Eastern Pacific during the 2006 spring season. Figure 1 also shows the location of ground based measurement stations including Mt. Bachelor (MBO) Oregon, Trinidad Head (THD) California, and Kathmandu (KTM) Nepal discussed later in this paper.

The modeled monthly mean CO distribution is shown in Fig. 2a. CO hotspots over much of Eastern China and India are seen at the 3 km AGL layer and the regions with enhanced CO extend north of ~10 N. A substantial amount of CO is seen entering the domain from Europe as shown along the northern boundary. Figure 2 also presents the mission wide averaged latitudinal and longitudinal CO distributions within the STEM modeling domain. Since STEM model was run on a Lambert Conformal projection, there are some latitudes and longitudes outside the model domain which are blank in the Fig. 2 subplots. The CO distribution along 45 N shows strong zonal transport with CO transported into the domain from Europe to Asia largely within the boundary layer as seen in the distribution in the western portion of the domain (i.e., <100 E longitude). CO from emissions in East Asia is transported out over the Pacific via frontal systems resulting in lifting of the CO above the boundary layer and into the free troposphere. The bulk of the CO transported is at altitudes of 4–5 km as shown in the cross section along 145 E longitude. As the polluted air masses reach the Eastern Pacific, the frontal systems tend to move pole ward, and aged air masses subside and mix with CO emitted from North America leading to enhanced CO levels within the boundary layer as shown in the 125 W cross section.

STEM model comparisons with observations from the DC-8 and C-130 flights are

ACPD
9, 16381–16439, 2009

also shown in Fig. 2. The predicted and DC-8 observation values for all flights are binned into every 1000 m flight altitude and then plotted. The horizontal error bars are the standard deviations of both model predictions and observations. The C-130 airborne observations and STEM model predictions are binned and averaged every 500 m in altitude. The CO predictions capture the main features in the observation, and predict values within 5–15% of observations, but with lower variability. The results show that the model underestimates observed CO for both the DC-8 and C-130 airborne observations. The model underpredicts CO at altitudes below ~5 km, to a greater extent for the DC-8 (~20 ppb, 15%) than for the C-130 flights (~7 ppb bias, 6%). At higher altitudes, the model shows a slight positive bias with respect to the DC-8 observations. The underestimation of CO could be attributed to several factors such as uncertainties in the anthropogenic and biomass emissions and chemical loss mechanisms some of which are discussed later in the paper.

The lifetime of CO in the atmosphere is about 1–2 months (Liang et al., 2004). Thus for 3-D modeling studies, it is useful to tag CO emissions from different source regions to help identify the source areas of a particular air mass. Figure 3 shows both the back trajectories and tagged CO tracer contributions to air sampled by the DC-8 and C-130 during INTEX-B. Three flights each from Hawaii (RF 11, 12, 13) and Alaska portions (RF 15, 16, 17) of the DC-8 mission were selected and 5-day back trajectories were calculated using the WRF meteorology for points along the flight paths. Similarly, five C-130 (RF 15, 17, 18 21, 24) flights that had substantial sampling over the Eastern Pacific were chosen to calculate back trajectories. The trajectories are initiated at the actual latitude, longitude, altitude and time of the airplane research flights. The trajectories were calculated along every minute of the flight path; however, to reduce the clutter in the Fig. 3, trajectories are plotted only every thirty minutes.

The back trajectory analyses show different transport patterns for the Hawaii and Alaska portions of the mission. The Hawaii portion is dominated by air masses passing over East Central China reaching as far back as South Asia. In Fig. 3, air mass trajectories are colored by the altitude along the trajectory, and as expected the higher

ACPD
9, 16381–16439, 2009

altitude air travels further reflecting the increase in wind speed with altitude. The back-trajectories for the C-130 show that the air-masses spent a substantial time over the Gulf of Alaska. In the tagged CO analysis, we track primary CO. To estimate total ambient CO levels, these enhancements would be added to a background concentration which is typically on the order of 90 ppb and accounts for the contribution to total CO from initial, top and lateral boundary conditions, biomass burning and net secondary production from chemical reactions. The tagged CO analysis shows that emissions from China contribute ~70% to the CO enhancements from anthropogenic emissions above background in these regions. The contribution from South and Southeast Asia is maximum in the mid/upper troposphere and reaches ~15%. At the higher latitudes associated with the DC-8 Alaska flights, there is a small contribution from South and Southeast Asia emissions. The contributions from USA and Canada sources range from 20–40% with the largest contribution at lower levels, reflecting the impact of offshore transport from North America during this season.

To evaluate the robustness of our trajectories and CO transport, we present the results for the meteorological variables simulated by the WRF model. The WRF model skill is evaluated for four key meteorological parameters essential for chemical transport with observations onboard the DC-8 and C-130 in Fig. 4. The values are binned and averaged according to the airborne altitude similar to CO results shown in Fig. 2. Figure 4a shows that the model is able to capture the vertical temperature profile quite well across all DC-8 flights. The standard deviation of the model and observed variables are also similar. The STEM meteorological pre-processor calculates relative humidity (RH) based on parameterized equations involving temperature pressure and water vapor mixing ratio. The WRF model captures the observed air pressure very well across all altitude bins (R~0.99, figure not shown, statistics presented in Table 1, supplementary material, see http://www.atmos-chem-phys-discuss.net/9/16381/2009/acpd-9-16381-2009-supplement.pdf). The comparison of RH is strictly not a robust evaluation of WRF model skill since it is based on the governing RH parameterized equation. However, since RH is an important parameter for chemical transport models,

ACPD
9, 16381–16439, 2009

we present the comparison. The results presented in Fig. 4b show that the model does fairly well in capturing the vertical distribution of the RH. The model shows a small positive bias in the lower troposphere and a larger negative bias in the upper troposphere. As shown in Fig. 4c, the WRF model captures the observed wind speed measured by the DC-8 flights up to six kilometer after which the model has a negative bias. For wind direction, the model shows low positive and negative bias across all flight altitudes (Fig. 4d). Similar results are found for the comparisons with the C-130 (Fig. 4e–h).

Figure 5a shows the monthly mean modeled ozone at the 3 km layer during the INTEX-B field campaign. Ozone results at the 3 km AGL shows hotspots over the Tibetan Plateau and the Eastern China. The results show a stronger latitudinal gradient over the Western Pacific compared to the Eastern Pacific. Compared to the monthly mean CO distribution, modeled ozone does not show as strong of an influence from the lateral boundary conditions coming from Europe.

Figure 5b and c show the modeled versus DC-8 and C-130 observations of ozone. The results show that the model is able to accurately capture the ozone vertical distribution for altitudes below 8 km; above which the DC-8 ozone is underestimated. The C-130 observations show that modeled ozone has a small negative bias (~3 ppb). Both the observations and the model show lower variability for the DC-8 flight locations than for the C-130 flights.

Figure 5d and e present the STEM-TUV model evaluation of the photolysis rates (J-value) for NO_2, a critical step in the formation of ozone. The calculation of J-NO_2 is complicated as it depends on the overhead column of ozone and the vertical distributions of ambient aerosol and clouds. Thus it is a good test of multiple parameter predictions. In general the model is able to capture the magnitude of observed NO_2 J-values. However, modeled J-NO_2 shows a general overprediction compared to observations, and a higher variability than observed.

To further test the consistency between the modeled and observed photochemical oxidant cycle we next compare nitrogen oxide distributions. Figure 6 presents the gas phase NO, NO_2 PAN and HNO_3 model vs. aircraft comparisons. The predicted values

ACPD
9, 16381–16439, 2009

of the sum of these four species capture many of the important features of the DC-8 and C-130 observations, including the vertical profiles and the enhancement in the C-130 values below 3 km. However the model overpredicts the sum by 20 to 70%. In terms of individual species both the model and observations show low NO_x concentrations above 3 km, and the model tends to overpredict NO_x in the boundary layer. PAN, a reservoir species of NO_x in the troposphere, is the most abundant species between 4 and 9 km. However the model overpredicts PAN by a factor of 2 at all altitudes. The second most abundant NO_y species above the boundary layer is HNO_3. The model underpredicts HNO_3 for both the DC-8 and C-130. The effect of heterogeneous reactions on gas phase nitric acid levels remains a source of uncertainty. Figure 6 also shows the profile assuming there is no partitioning of nitric acid to aerosols, calculated by adding the particulate nitrate back to the gas phase in the form of HNO_3. This improves the prediction of gas phase HNO_3 when compared with observations, but exacerbates the overprediction of NO_y.

Zhang et al. (2008) used OMI NO_2 to constrain NO_x emissions and they were able to capture the NO_x observations from DC-8 and C-130 using the GEOS-Chem model. Their reported emissions are similar to those we used for China, Korea and Japan. However, we have used higher South and South-East Asian NO_x emissions than used by Zhang et al. (2008). As we will discuss later NO_x emissions from South East Asia differ from the TRACE-P emissions inventory by as much as 80% while South Asia emissions differed by 20%. For the C-130 observations it is important to note that we have used NO_x emissions from NEI-2001 as compared to NEI-1999 which was used in the Zhang et al. (2008) GEOS-Chem analysis. Therefore, these emissions inventories need to be re-evaluated along with the NO_y chemistry for model improvement. Also as discussed later in the paper, top and lateral boundary conditions influence modeled PAN. In our simulations, the impact of boundary conditions is substantial as discussed later in the paper (Sect. 4).

Figure 7 compares observed and predicted OH and the ozone photolysis rate constant (J-O_3) from the DC-8 and C-130 flights. The modeled OH shows a positive bias

ACPD
9, 16381–16439, 2009

at lower altitudes and negative bias at high altitude when compared to the DC-8 observations. Modeled OH values are much closer to the C-130 OH observations than the DC-8. The J-O_3 values and vertical profiles are accurately calculated, but with a negative bias in the upper atmosphere for the DC-8. Above 5 km the RH values were also underpredicted. This coupled with the low J-O_3 values can help explain the underprediction of OH above 5 km for the DC-8. Predicted HO_2 vertical profiles are consistent with the observed distribution for both the DC-8 and C-130, but with a systematic underprediction. HO_2 formation is initiated by the reaction of CO with the OH radical which also leads to formation of hydrogen peroxide. Hydrogen peroxide is highly soluble with water and therefore is efficiently removed by wet deposition. Our modeled values of hydrogen peroxide concentrations and its photolysis rates (J-H_2O_2) compare well with the aircraft observation (Figure not shown, statistic presented in Tables 1 and 2 of the supplemental materials).

Mao et al. (2008) analyzed the HO_x measurements from the DC-8 platform during the INTEX-B mission (Mao et al., 2008). They compared the DC-8 airborne measurements with NASA Langley box model prediction of OH. They concluded that the overprediction of OH in the boundary layer by the box model is related to underprediction of modeled formaldehyde (HCHO) when compared with measured HCHO aboard the DC-8. Our model, which has a different chemical mechanism, is used to test this hypothesis. There were two independent measurements of HCHO onboard the DC-8. We present the model comparison with observations for both measurements in Fig. 7d and h. While the model versus one of the measurement sets (i.e., NCAR-formaldehyde) seems to supports this hypothesis the other measurement (i.e., URI-formaldehyde) does not. At the present it is not clear from the HCHO measurement-STEM comparison if the above hypothesis is correct or not. However, it must be kept in mind that the differences in the averages between the two HCHO measurements and between each measurement and the model are all within the quoted measurement uncertainties. While overprediction of STEM modeled OH with DC-8 OH observations may explain some of the underprediction of CO at the boundary layers, consistent with the hypothesis of Zhang et al. (2008),

ACPD
9, 16381–16439, 2009

it is not able to explain the CO underprediction with the C-130 observations.

3.1 Spatial distribution of aerosols

Monthly averaged horizontal distributions of aerosols show strong zonal patterns with the bulk of the aerosol confined between 10 to 50 N as shown in Fig. 8. The dust distribution shows maximum values in the western part of the domain reflecting the strong source regions during this time period (i.e., Central Asia and China). The sulfate distribution shows a strong west to east gradient, with the peak values in the west reflecting the heavy populated and industrial regions of India and China. OC shows a similar pattern, but with elevated levels also over Southeast Asia, reflecting the importance of biomass burning. Particulate nitrate shows a different pattern, with elevated levels over South Asia and a large region extending across the Pacific. These patterns generally reflect regions with high NO_x and NH_3 emissions.

The comparison of observations to modeled aerosols along the flight tracks is challenging as the aerosols are transported in relatively discrete plumes across the Pacific. Dunlea et al. (2008) reported that for some of the flights during INTEX-B, the models missed transport of large polluted air masses that were so intense that missing these concentrations could easily modify the average vertical profiles of aerosols. Figure 9 presents the comparison of model predicted and observed aerosols from the DC-8 and C-130. For the C-130 observations, we compare only to the AMS data but Dunlea et al. (2008) showed that the AMS and PILS instrument measured similar concentration of nitrate and sulfate during the INTEX-B study. The predicted sulfate values are generally well captured for the DC-8 flights in terms of both mean values and variability (e.g., both the model and observations show the largest variability in 1 to 4 km altitude range). However, the model fails to capture the elevated sulfate levels above 2 km that were observed by the C-130. In addition the predicted variability is also much lower than the observations. Evaluation of modeled SO_2 with both DC-8 and C-130 observations (showed in Fig. S1 and Tables S1 and S2 of the supplemental materials) shows that SO_2 is systematically underpredicted by the model. Thus, it seems that the cur-

ACPD
9, 16381–16439, 2009

rent emission inventory may be low on SO_2 emissions. However, the predicted results below 2 km for both the DC-8 and C-130 are well captured for both sulfate and SO_2. The large underpredictions in the mid troposphere for the C-130 may reflect other issues related to transport and removal of sulfur compounds in the model. The nature of the pollutant transport in discrete plumes across the Pacific could also contribute significantly to the underprediction of modeled SO_2 and sulfate.

The comparison of nitrate aerosols from the DC-8 shows that the model overpredicts the nitrate concentration at lower altitudes while it underpredicts nitrate aerosols at higher altitudes. However as shown in Fig. 6, the modeled HNO_3 gas phase values are underpredicted, but total nitrate (gas + particulate nitrate) is well captured. This suggests that the partitioning in the model to particulate phase on dust, sea salt and potassium maybe too strong. The HNO_3 partitioning between gas phase and particulate phase needs to be analyzed further using a box model study constrained with observations. Model comparison of nitrate aerosols with the C-130 measurement shows that the model overpredicts the observation at all altitudes although the overprediction is smaller at higher altitudes.

While the AMS instrument onboard the C-130 measures organic aerosols, the STEM model calculates concentration of primary organic carbon only. Thus, comparison of modeled OC with AMS organic matter (OM) is complex. However, if one were to convert AMS OM to OC with the OM/OC ratio of 1.9 reported for this study (Dunlea et al., 2008) and which is consistent with values for rural and remote aerosols reported elsewhere (Turpin and Lim, 2001; Aiken et al., 2008) our model underpredicts the observations, consistent with missing SOA formation and the importance of SOA to global OA highlighted by previous studies (e.g. Volkamer et al., 2006; Zhang et al., 2007; Hallquist et al., 2009). If we assume that the difference between the observed and predicted OC is due to secondary organic aerosol (SOA), then SOA accounts for about 40% of the OC. We present the results of AMS OM converted to OC with our model prediction in Fig. S2 and Table S2 of the supplemental materials for discussion of aerosol transport across the Pacific discussed in the next several paragraphs.

ACPD
9, 16381–16439, 2009

Modeling studies allow analysis of pollutant evolution as air masses are transported away from the source regions. Figure 10 shows the mission wide averages of calculated sulfate, potential sulfate (SO_2 + sulfate) and VOC age (Tang et al., 2004a). The VOC age is a relative clock and gives qualitative information on the age of air masses, and can be made more quantitative by calibration with other air mass age indicators (e.g., trajectory analysis). The VOC age calculations are done with the modeling domain without boundary conditions so that the VOC inferred age at the western boundary is young. We present the results at 45 N latitude because most of the C-130 Pacific flights occurred between 40–50 N latitude as seen in Fig. 1. Our results show that as we move east there is a distinct sulfate plume extending from about 3 to 7 km. In addition there is a second sulfate peak at similar altitudes associated with the North America plume located around 130 W. Also plotted is the calculated sulfate to potential sulfate ratio (i.e., the sum of sulfate plus SO_2 expressed as sulfate) ratio, which shows that the portion of available sulfur in the form of sulfate increases across the Pacific, consistent with SO_2 transformation to sulfate as it advects eastward to North America. Modeled results show that as air masses approach the North American continent, the ratio of sulfate to potential sulfate decreases at the lower altitudes signifying the influence of North American SO_2 emissions on the air mass. However we also see regions within the boundary layer extending from 130 W to 150 E with ratios greater than 0.8, reflecting the fact that air masses reaching near the surface can have very long residence times. This is more clearly seen in the plot of VOC air mass age. The aging of the air masses as they are transported to the east is clearly seen, with air in the upper troposphere taking on average 6 to 8 days to reach North America, a duration similar to that found in previous studies (Jaffe et al., 1999; Reidmiller et al., 2009). Furthermore air masses near the surface over the Pacific can have ages exceeding 10 days. A clear delineation between North America outflow and long range transport for Asia is seen at 130 W. The VOC age has a similar distribution as the sulfate to potential sulfate ratio (as expected as this is another chemical clock). Note that the distributions of VOC age and the ratio of sulfate to potential sulfate distribution are similar east of

ACPD
9, 16381–16439, 2009

100 E. West of 100 E the sulfate to potential sulfate ratio is large reflecting the fact that the inflow boundary conditions bring in aged air masses from the western boundary. STEM model results based on monthly mean OC and sulfate mixing ratios agree with Peltier et al. (2008) C-130 observations in that up to an altitude of ~3 km the ratio of OC/sulfate is about 1 or higher. As we follow the Asian air mass (from VOC age or from the sulfate/potential sulfate ratios) we found that the ratio declines as we move up in altitude to values ~0.4, which is also consistent with the observations.

It is interesting to point out that the mean sulfate distribution does show an enhancement in sulfate in the region where the C-130 operated. While the model extraction at the time and locations of the actual flights show only a slight enhancement in sulfate in the 2–7 km altitude range (Fig. 9a), a displacement of the predicted feature slightly to the west would be consistent with the observations. As discussed earlier with respect to the predicted meteorology, the negative bias in the wind speed above ~5 km could have resulted in a slight displacement in longitude and latitude of the mean distributions.

Using these results we also examined the modeled OC to sulfate ratios as this has been discussed previously by Dunlea et al. (2008) and Peltier et al. (2008) for the same INTEX-B campaign. The OC to sulfate ratio reflects the differences in emissions, wet removal, and formation processes. Dunlea et al. (2008) compared organic carbon (converted from OM measurements) ratio with AMS sulfate, while Peltier et al. (2008) examined the water soluble organic carbon (WSOC) with sulfate aerosols using their PILS instrument. Both studies compared the aerosol ratios of organic carbon to sulfate with their own separate definitions of Asian air mass origin to elucidate the transport and transformation of aerosols across the Pacific. Dunlea et al. (2008) identified air masses of Asian origin using observed AMS sulfate >1 μg/m^3 and included only those data sampled by the C-130 west of 125 W degrees longitude. Peltier et al. (2008) screened data for Asian CO greater than 75% of the total anthropogenic Flexpart CO as air masses originating from Asia. The STEM modeled values were examined using the data screening criteria defined by Dunlea et al. (2008). We also

ACPD
9, 16381–16439, 2009

classified the STEM model data similar to Peltier et al. (2008) study using predicted CO greater than 100 ppb and tagged China anthropogenic CO greater than 50% of the predicted total anthropogenic CO as screening criteria. Dunlea et al. (2008) showed that AMS and PILS instrument both showed similar results for sulfate concentration. We used AMS sulfate and AMS OC (calculated from OM) data for comparison as it was readily available for both Peltier et al. (2008) and Dunlea et al. (2008) screening techniques mentioned above. The OC to sulfate ratios screened in these ways are shown in Fig. 11. Also shown are the OC to sulfate ratios for all the data points for the C-130 flights (no screening). Using all the data the OC to sulfate ratio is approximately 1 in the lowest 3 km, and drops to a value of ~0.3 at altitudes between 3 to 6 km. The Peltier screening method shows a similar altitude dependency of the OC to sulfate ratio, with lower values (~0.6) in the lower altitudes. This is the result of their screening method that removes some of the freshest air masses from North America (which occur in the lowest 3 km and which have higher OC to sulfate ratios). The Dunlea screening method looks only at air massed that have large enhancements of Asian pollution. It removes the North American air masses as well as Asian air masses that have low pollution contributions. Their results show a different vertical profile with the lowest values (<0.2) occurring near the surface, and increasing to ~0.3 at 3 km. Above 3 km the value remains at ~0.3. At altitudes above 4 km all the profiles show that the ratio is of order 0.3–0.4.

The STEM predicted OC to sulfate ratio profiles for the various screening methods are also shown in Fig. 11. The magnitude of the OC/SO_4 ratio from the STEM model is larger than the corresponding observed AMS ratio. This may be due to the substantial underprediction of sulfate aerosol, although OC is also underpredicted as discussed above. The sulfate and OC profiles for the data screened by Dunlea et al. (2008) and Peltier et al. (2008) criteria are shown in Figs. S3 and S4 of supplemental materials. While the absolute ratios are biased high, the predicted profiles capture the important features of the observation based ratios. For example the impacts of the various screening methods on the profiles are clearly shown. The Peltier method results in a

ACPD
9, 16381–16439, 2009

reduction of the ratios at all altitudes, with the greatest differences in the lower 2 km. The Dunlea screening results in a greater reduction in the ratios. These results can be understood in the context of the information presented in Fig. 10 and its discussion. Both screening techniques remove contributions of OC and sulfate of North American origin. The criteria used by Dunlea removes a substantially larger fraction of the North America contribution. The low values near the surface in the Dunlea screening is due to the fact that these observation points are very aged as reflected in the monthly mean air mass age distributions shown in Fig. 10c. These results support the idea that the OC to sulfate ratio is lower in more aged air masses. However, these results should be interpreted cautiously. Peltier et al. (2008) compared WSOC/sulfate ratios while we compared OC/sulfate ratios. Our results show that Asian air mass classified according to observed Asian tracers show different altitude profile than modeled monthly mean ratios. Results based on observation sampling strategy, which is biased towards sampling polluted plumes, could also influence the results of aerosol transport and transformation compared to monthly/seasonal mean values.

3.2 Comparison with surface observations

Observations of trace gases and aerosols were also available from surface sites at Mt. Bachelor (MBO) and Trinidad Head (THD) during the INTEX-B sampling period. The comparison of predicted CO, Ozone, NO and PAN with measurements from Mt. Bachelor during the INTEX-B is shown in Fig. 12. Apart from the first few days of the comparison, the model is able to capture the magnitude and variation of measured CO at Mt. Bachelor. The model is also able to capture both the magnitude as well as the temporal trend of ozone and PAN. Modeled NO is within the range of observed values but shows less variability. It is important to note that modeled PAN is much closer in agreement to the measurements at Mt. Bachelor than when compared to the airborne DC-8 and C-130 measurements. The predictions also accurately capture the three synoptic events observed in this period. Figure 13 shows the curtain plots of ozone, PAN and dust over Mt. Bachelor illustrating the vertical distribution of these pol-

ACPD
9, 16381–16439, 2009

lutants. The ozone curtain shows strong influence of stratospheric ozone throughout the INTEX-B period. PAN vertical structure shows influence of local sources as well as elevated plumes associated with long range transport. Dust shows a somewhat different vertical distribution over Mt. Bachelor, with three distinct events passing over Mt. Bachelor. The peak in the dust concentration is located 3–8 km AGL. The superimposed figure of modeled surface level dust, ozone and PAN shown in Fig. 13, illustrates the different characteristics of these three pollution events. The first peak around 22 April has very high ozone concentration and relatively low PAN (with peak ozone being anti-correlated with PAN), and low dust values. The second peak around 3 May has both high ozone and PAN but low dust concentration. Finally the peak around 11 May has high ozone, dust and PAN.

To help put these measurements in perspective modeled ozone, PAN and dust distribution at 3 km AGL at 18 Z for 22 April, 3 and 11 May are shown in Fig. 14. Wind barbs are also plotted in these figures to illustrate the transport patterns. On 22 April, modeled ozone is high over MBO along the eastern side of the ridge bringing descending air of stratospheric origin from the North. The ridge clearly separates the ozone transported from Asia which is on the western side of the ridge. Thus the air over MBO has high ozone and low dust as shown clearly in the vertical profiles in Fig. 13. On 3 May, there is another weak ridge over the Eastern Pacific which transports pollution from the North. This ridge is not as strong as on 22 April. To the east of the ridge ozone and PAN are correlated, with maximum values at the surface, and moderate values aloft. Dust values at the surface remain low, reflecting the lack of local emissions and wet removal along its transport path. The third pollutant peak over MBO around 11 May shows zonal flow transporting dust, ozone, PAN and other pollutants from Asia to the west coast of the US.

To further understand the characteristics of these three pollutant events from source origin perspective, the observed data of selected chemical species were combined with the air mass back trajectories. For this analysis, we used 12 day backward trajectories calculated from the model to assess the impact of long range transport over MBO.

ACPD
9, 16381–16439, 2009

The location of an air parcel at a particular time was represented by the trajectory segment endpoints as latitude and longitude. The entire geographic region covered by the trajectories was divided into an array of grid cells. It was assumed that the concentration did not change from the value observed at MBO for a particular time along the back trajectories. Let $m_{i,j}$ be the number of segment endpoints in *i,j*-th grid cell that denote the trajectories arriving at MBO when the time corresponds to a particular pollution event described above. The average concentration of each grid cell $C_{i,j}$ was calculated by using the Eq. (1):

$$C_{i,j} = \frac{1}{m_{i,j}} \sum_{k=1}^{m_{i,j}} C_k \quad (1)$$

where C_k denotes the observed concentration at the time when the back trajectory was initialized. Thus the concentration of species was reconstructed along the path of back trajectories. Further details are explained in Kurata et al. (2004). The trajectories were colored by the mean observed pollutant concentration associated with them and these results are also shown in Fig. 14. The reconstructed concentration plot of ozone along the trajectory path for the first event around 22 April clearly shows the path of the high ozone (grid cells colored in red) coming from the north with relatively lower values along the Asian transport path. Similar plots for PAN and dust (not shown here) show low values consistent with the above findings. Like wise, plot of PAN for the second peak event on 3 May shows that high values of PAN and ozone (not shown) with relatively lower dust (not shown) originate along the path coming from the north/northwest direction. Finally for the third peak of 11 May, the dust plot clearly shows that the high values of dust, along with PAN and ozone (not shown) are transported along the zonal flow originating from Asia. These results corroborate the findings discussed above.

To further understand the emission source regions that influence the pollution levels at MBO, tagged tracer analysis was performed. Figure 15 shows the time series of source region tagged anthropogenic CO over MBO at the 5.3 km AGL and at the surface. Connecting these two figures, we show the modeled CO curtain over MBO.

ACPD
9, 16381–16439, 2009

China CO and continental US (CONUS) CO dominate the source regions during this period, with the importance of China sources increasing with altitude. The tagged CO tracer study also corroborates the earlier finding that the first two peak events have pollutants coming from the North (as shown by elevated Canada CO tracer) while the last pollutant event is transported more zonally from Asia.

Aerosol mass measurements were also available from the Atmospheric Brown Cloud (ABC) sites at Trinidad Head (THD) and Kathmandu, Nepal (KTM) during the INTEX-B field campaign. We present the model comparison of aerosol mass at THD with observations, modeled aerosol curtain plots over THD and comparison of modeled and observed aerosol mass at KTM in Fig. 16. Aerosols were sampled every day in KTM while sampling was done every other day in THD. The results show that the model is able to capture the magnitude of the total $PM_{2.5}$ mass at THD with some underprediction during the first week. Modeled sulfate is also lower than observed at THD consistent with the comparison of predicted values with the airborne measurements from the DC-8 and C-130. The general trends are captured except for the episode around 1 May, which was missed by the model. The model does predict elevated sulfate over THD during this time period, but only for altitudes above 4 km. The OC concentrations are within the magnitude of the observations at THD, unlike the airborne comparison where the STEM model was significantly underpredicting observed OC inferred from AMS OM measurements. At KTM, modeled $PM_{2.5}$ mass concentration and variability are well captured. Modeled sulfate levels are also similar to the observations while the modeled OC is underpredicted. The underprediction of OC is likely attributable to local emission sources which are not captured by the regional emissions inventory used in this study. The OC underprediction could also have resulted from the lack of secondary organic formation mechanism in the STEM model.

The INTEX-B campaign with the DC-8 and C-130 aircrafts was designed to be executed such that pollutant ageing could be studied by conducting quasi lagrangian sampling of air masses between the two aircrafts (Singh et al., 2009). Fuelberg et al. (2008) used backward and forward trajectories between the C-130 and the DC-8 to

ACPD
9, 16381–16439, 2009

help indicate where such lagrangian sampling might have occurred. We extended this analysis to include the surface sites. Figure 17 illustrates the backward and forward trajectories from one C-130 flight with the DC-8 and the surface sites of Mt. Bachelor and Trinidad Head meeting our criteria for lagrangian sampling. Supplemental materials include the tables (S3, S4, S5, and S6) that present the detailed times and location from the DC-8 and C-130 to the two surface sites where model calculated lagrangian sampling occurred. We include only the results for air masses that arrived more than a day later at the surface sites to avoid counting the air masses where the C-130 flew directly over or near these surface sites. To illustrate how this information can be used, we analyzed one case of quasi-lagrangian sampling between the two airborne platforms which was later sampled at the two surface sites. Figure 17 illustrates the position of the DC-8 and C-130 for the case we analyzed. For these particular trajectories the passing heights over the surface sites are between 3–4 km as shown in the curtain plots for MBO and THD (Figs. 12, 14 and 15). The C-130 was ~1 day down wind of the DC-8 observations and MBO and THD were ~2 days downwind of the C-130. For the trajectories connecting the DC-8, C-130 at MBO, the observed CO concentrations were ~120 ppb while the O_3 values were ~50 ppb. However, for the trajectories connecting the DC-8, C-130 and THD, the sulfate aerosol increased from ~0.3 μg/m^3 to ~0.6 μg/m^3, to ~1.5 μg/m^3, respectively.

3.3 Summary of comparison with aircraft observations

A mission-wide summary of the model predictions compared to the observations is presented in Tables 1 and 2 of the supplemental materials. Observed and modeled species mean values, standard deviation, and correlation coefficient, R, are presented. Plots of the ratio of observed to predicted mean values (Fig. 18) show that for most parameters, the predicted values are within a factor of 2 (or better) of the observations. The largest differences occur for nitric acid (underpredicted) and particulate nitrate (overpredicted), and we believe this is related to the calculation of partitioning as discussed previously. In a previous study we found that during the TRACE-P mission that

ACPD
9, 16381–16439, 2009

the STEM model reproduced observations better at lower altitudes (Carmichael et al., 2003). For INTEX-B, we do not see as strong of an altitude dependence in the model skill. Results from the same analysis for TRACE-P showed no apparent bias towards meteorological variables, gas phase species or aerosols. However, the current study shows a scatter with altitude. Current results also show that meteorological variables are generally better predicted than gas phase species, which in turn are predicted better than aerosol quantities. The R values for photolysis rates (J) are similar for gas phase species. The scatter in R values is expected as the air masses have time to mix and reach background levels as they advect eastward. The low R values for all aerosols in comparison to meteorological variables and gas phase species illustrate the uncertainties of aerosol emissions and removal processes in the model.

4 Sensitivity studies

Asian emissions have changed substantially over Asia from 2000 to 2006 (Zhang et al., 2009). Table 6 in the paper by Zhang et al. (2009) summarizes the changes in emissions for some of the anthropogenic trace gases and aerosols throughout Asia. NO_x emissions have changed the most over all of Asia with higher emissions from all source regions. SO_2 emissions have also grown substantially over China, but have decreased over Korea/Japan (other East Asia). South Asia shows a growth of 24% in SO_2 emissions from the year 2000 to 2006. Carbonaceous aerosol emissions in China have grown substantially, while South Asian emissions are lower in 2006, reflecting an overestimation in the 2000 inventory.

Figure 19 shows the changes in the distribution of emissions in our modeling domain for CO, and BC from the TRACE-P to INTEX-B campaigns (positive values reflect that 2006>2000 emissions). To see the impact of changes in emissions on the trace gas distributions over the Pacific, an additional calculation was performed using the Trace-P emissions (but the meteorology for the INTEX-B period). The impact of the emission changes from TRACE-P to INTEX-B is to increase monthly mean values over

ACPD
9, 16381–16439, 2009

the Eastern Pacific by 1–5 ppb of CO and 0.05–0.1 $\mu g/m^3$ of BC.

The importance of biomass burning emissions was evaluated by comparing simulation results with and without the inclusion of the biomass burning emissions (Fig. 19). Biomass burning emissions contribute 10–20 ppb to the monthly mean of CO over the DC-8 and C-130 sampling areas. Al-Saadi et al. (2008) analyzed four different satellite based biomass emissions estimate technique and concluded that the emissions varied by a factor of 10 (Al-Saadi et al., 2008). Since the STEM model is underpredicting the CO concentration when compared to airborne observations, biomass CO may provide the missing link. This is a subject for future analysis.

Boundary conditions are another source of uncertainty in regional chemical model calculations. This is shown in Fig. 20 where we present model calculations based on two different sets of global model boundary conditions. In one calculation we used RAQMS model forecast predictions for our boundary conditions; for the other we used "post analysis" MOZART model boundary conditions. The results show that for long lived species such as ozone and PAN, the regional predictions are sensitive to the boundary conditions, while for shorter lived species such as aerosols, the regional predictions are insensitive.

We also examined the importance of heterogeneous chemistry on the trace species distributions during INTEX-B. Heterogeneous chemistry on dust surfaces was shown to be important during the Trace-P and ACE-Asia field campaigns by Tang et al. (2004). An additional simulation was performed where the reactions of ozone, SO_2 and NO_2 and HNO_3 on dust were turned off. The change in trace species distributions are presented in Fig. 21. In the East Asia outflow the impact of heterogeneous reactions on dust is significant, increasing the average aerosol sulfate and nitrate by up to 10% and 20%, respectively, while reducing ozone levels by 5 to 10%. Over the Central and Eastern Pacific, where the INTEX-B flights were conducted, the mean impacts of the heterogeneous reactions on dust for sulfate and nitrate were 1–5%.

However the impacts of the heterogeneous reactions at specific times during dust transport episodes can be significant. McNaughton et al. (2009) analyzed the aerosol

ACPD
9, 16381–16439, 2009

and gas phase measurements on the DC-8 aircraft to show that in the presence of dust both sulfate and nitrate aerosol production is increased, and that as a result of the dust reactions, gas phase nitric acid levels are reduced appreciably. In Fig. 22a we show plots of observed sulfate to total potential sulfate (sum of sulfate and SO_2) as a function of aerosol Ca for all DC8 flights, for altitudes above 1.5 km, CO and O_3 greater than 90 and 40 ppb, respectively along with ^{7}Be less than 800 fCi s/m^3 to exclude data influenced by clean air masses and stratosphere. The data points show an envelope, with the ratio increasing with increases in Ca. Also shown are the predicted values for the ratio plotted as a function of predicted dust concentration. The model shows a very similar behavior. In Fig. 22b, d we plot the observed and modeled ratio of particulate nitrate to total nitrate (sum of particulate nitrate and gaseous nitric acid). Observations show that for Ca concentrations above ~0.5 μg/m^3, the nitric acid partitions into the dust, reducing the gas phase concentrations by ~50% (as discussed further in McNaughton et al., 2009). The model shows qualitatively a similar behavior.

We also evaluated the importance of aerosols on the photochemistry over the Central and Eastern Pacific through their impact on photolysis rates. For this simulation we turned off the effect of aerosols in the TUV photolysis model (i.e. made the aerosol concentration values equal to zero in the TUV subroutine). Figure 23 shows the percent change in the mean concentrations of OH, ozone, NO_x and sulfate aerosol due to changes in the photolysis rate calculation for the Hawaii portion (16–30 April) of the INTEX-B campaign. Our results show that aerosols strongly influence the chemistry of short lived species like OH and NO_x over the polluted regions of Asia and the Western Pacific. However, the effects on average are small over more remote regions such as the Central and Eastern Pacific.

5 Summary

STEM, a regional chemical transport model was used to simulate the outflow of aerosols and trace gases from Asia to North America during the spring of 2006.

The model performance was evaluated with observations from the NASA INTEX-B field campaign. The STEM chemical transport was driven by the recently developed Weather Research and Forecast (WRF) meteorological model. Results from the WRF model showed that it was able to capture the meteorological variables adequately to simulate chemical transport. Furthermore, STEM model evaluation showed that it was able to capture the magnitude of the aerosols and trace gases within a standard deviation of most of the observed mean values. Despite successfully predicting many observed species such as observed ozone in the DC-8 flights, the results point towards areas where model improvements are needed. The STEM model underestimated CO whereas it overpredicted PAN. The errors in the model calculations are attributed to uncertainty in emissions estimates and uncertainty in the top and lateral boundary conditions. Comparison of STEM model OH concentrations with two independent formaldehyde observations from the DC-8 emphasizes the need for further HCHO measurement comparisons with instruments having even lower uncertainty limits for establishing a clear link for OH overprediction to simulated underprediction of formaldehyde.

The modeling results show that during the INTEX-B campaign, transport pathways of gaseous species and aerosols were different. While most of the long lived trace gas concentrations showed a north/south gradient over the Pacific, the aerosol transport pathway was mostly between 30–40 N latitude.

Comparison of modeled sulfate to airborne observations showed that the model underestimates the magnitude of sulfate concentration in the Eastern Pacific. This appears to be due to an under estimation of sulfur emissions and a transport-related displacement of the predicted location of the mid-tropospheric peak in sulfate. STEM modeled pollutant concentration values were also compared with measurements made at two surface sites: Mt. Bachelor, Oregon and Trinidad Head, California. The model is able to adequately capture the magnitude and synoptic variations of trace gases and aerosols at both these sites. The results from Kathmandu, Nepal shows where model improvements are needed to represent South Asian outflow.

ACPD

9, 16381–16439, 2009

Modeling experiments were performed to evaluate the impact of increasing Asian emissions from 2000 to 2006 over the Pacific and North America. The contribution of biomass burning on observed CO and carbonaceous aerosol concentration was presented along with the outflow transport path. Mission wide average modeled aerosol and trace gases distribution were presented to put the airborne observations in perspective as most of the airborne sampling was designed to capture higher concentrated pollutant plumes. Tagged CO tracer studies along with back trajectory analysis were performed to identify the source regions of observed pollutants.

The impact of heterogeneous chemistry on dust surfaces was also evaluated. The results showed that these mechanisms are important and in dust laden air masses can enhance the production of aerosol sulfate and nitrate, and significantly reduce the nitric acid concentrations over the Central and Eastern Pacific. Modeled results showed that while aerosol contributions to photolysis rate calculations were important over the source region, they were not significant over the Central and Eastern Pacific for the two week INTEX-B period.

These results show that chemical transport models provide an important tool for the analysis of comprehensive data sets such as that obtained in INTEX-B. However there remain important limitations. For example, this study pointed out problems in the prediction of HO_2, PAN, the gas-particle partitioning of nitric acid, and sulfate over the Western USA. Further improvements in the models will require better estimates of emissions, a better understanding of aerosol-gas phase interactions, and a better understanding of the root causes of errors in the prediction of important aspects of the photochemical processes (model deficiencies or something else?).

Acknowledgements. We would like to thank the INTEX science team. This work was supported by a NASA grant (NNG04GC58G and INTEX-B). The heterogeneous chemistry portion was based on work done under a NSF grant (0613124). The authors would also like to acknowledge NOAA and Atmospheric Brown Cloud project for support of the Trinidad Head and Kathmandu measurements.

References

Aiken, A. C., DeCarlo, P. F., Kroll, J. H., et al.: O/C and OM/OC Ratios of Primary, Secondary, and Ambient Organic Aerosols with High Resolution Time-of-Flight Aerosol Mass Spectrometry, Environ. Sci. Technol., 42, 4478–4485, doi:10.1021/es703009q, 2008.

Al-Saadi, J., Soja, A., Pierce, R. B., Szykman, J., Wiedinmyer, C., Emmons, L., Kondragunta, S., Zhang, X. Y., Kittaka, C., Schaack, T., and Bowman, K.: Intercomparison of near-real-time biomass burning emissions estimates constrained by satellite fire data, J. Appl. Remote Sens., 2, 021504, dio:10.1117/1.2948785, 2008.

Bertschi, I. T., Jaffe, D. A., Jaegle, L., Price, H. U., and Dennison, J. B.: PHOBEA/ITCT 2002 airborne observations of transpacific transport of ozone, CO, volatile organic compounds, and aerosols to the northeast Pacific: Impacts of Asian anthropogenic and Siberian boreal fire emissions, J. Geophys. Res.-Atmos., 109, D23S12, doi:10.1029/2003JD004328, 2004.

Bey, I., Jacob, D. J., Logan, J. A., and Yantosca, R. M.: Asian chemical outflow to the Pacific in spring: Origins, pathways, and budgets (106, 23097–23113, 2001), J. Geophys. Res.-Atmos., 108(D5), 4162, doi:10.1029/2003JD001603, 2003.

Carmichael, G. R., Peters, L. K., and Kitada, T.: A 2nd Generation Model for Regional-Scale Transport Chemistry Deposition, Atmos. Environ., 20, 173–188, 1986.

Carmichael, G. R., Tang, Y., Kurata, G., Uno, I., Streets, D., Woo, J. H., Huang, H., Yienger, J., Lefer, B., Shetter, R., Blake, D., Atlas, E., Fried, A., Apel, E., Eisele, F., Cantrell, C., Avery, M., Barrick, J., Sachse, G., Brune, W., Sandholm, S., Kondo, Y., Singh, H., Talbot, R., Bandy, A., Thorton, D., Clarke, A., and Heikes, B.: Regional-scale chemical transport modeling in support of the analysis of observations obtained during the TRACE-P experiment, J. Geophys. Res.-Atmos., 108, 8823, doi:8810.1029/2002JD003117, 2003.

Carter, W. P. L.: Development and evaluation of the SAPRC-99 chemical mechanism, final report to California Air Resources Board, Air Pollution Research Center and College of Engineering Center for Environmental Research and Technology, University of California, Riverside, CA, USA, Contract No. 92–329, 2000.

Dunlea, E. J., DeCarlo, P. F., Aiken, A. C., Kimmel, J. R., Peltier, R. E., Weber, R. J., Tomlison, J., Collins, D. R., Shinozuka, Y., McNaughton, C. S., Howell, S. G., Clarke, A. D., Emmons, L. K., Apel, E. C., Pfister, G. G., van Donkelaar, A., Martin, R. V., Millet, D. B., Heald, C. L., and Jimenez, J. L.: Evolution of Asian aerosols during transpacific transport in INTEX-B, Atmos. Chem. Phys. Discuss., 8, 15375–15461, 2008,

http://www.atmos-chem-phys-discuss.net/8/15375/2008/.
Fuelberg, H. and Latto, A.: Quasi-Lagrangian Sampling during INTEX-B: http://fuelberg.met.fsu.edu/research/intexb/intersect/desc.html, 2008.
Garg, A., Shukla, P. R., and Kapshe, M.: The sectoral trends of multigas emissions inventory of India, Atmos. Environ., 40, 4608–4620, 2006.
Gong, S. L.: A parameterization of sea-salt aerosol source function for sub- and super-micron particles, Global Biogeochem. Cy., 17, 1097, doi:1010.1029/2003GB002079, 2003.
Grassian, V. H.: Chemical reactions of nitrogen oxides on the surface of oxide, carbonate, soot, and mineral dust particles: Implications for the chemical balance of the troposphere, J. Phys. Chem. A, 106, 860–877, 2002.
Hadley, O. L., Ramanathan, V., Carmichael, G. R., Tang, Y., Corrigan, C. E., Roberts, G. C., and Mauger, G. S.: Trans-Pacific transport of black carbon and fine aerosols (D<2.5 μm) into North America, J. Geophys. Res.-Atmos., 112, D05309, doi:05310.01029/02006JD007632, 2007.
Hallquist, M., Wenger, J. C., Baltensperger, U., Rudich, Y., Simpson, D., Claeys, M., Dommen, J., Donahue, N. M., George, C., Goldstein, A. H., Hamilton, J. F., Herrmann, H., Hoffmann, T., Iinuma, Y., Jang, M., Jenkin, M., Jimenez, J. L., Kiendler-Scharr, A., Maenhaut, W., McFiggans, G., Mentel, Th. F., Monod, A., Prévôt, A. S. H., Seinfeld, J. H., Surratt, J. D., Szmigielski, R., and Wildt, J.: The formation, properties and impact of secondary organic aerosol: current and emerging issues, Atmos. Chem. Phys. Discuss., 9, 3555–3762, 2009, http://www.atmos-chem-phys-discuss.net/9/3555/2009/.
Jacob, D. J., Crawford, J. H., Kleb, M. M., Connors, V. S., Bendura, R. J., Raper, J. L., Sachse, G. W., Gille, J. C., Emmons, L., and Heald, C. L.: Transport and Chemical Evolution over the Pacific (TRACE-P) aircraft mission: Design, execution, and first results, J. Geophys. Res.-Atmos., 108, 1–19, 2003.
Jaffe, D., Anderson, T., Covert, D., Kotchenruther, R., Trost, B., Danielson, J., Simpson, W., Berntsen, T., Karlsdottir, S., Blake, D., Harris, J., Carmichael, G., and Uno, I.: Transport of Asian air pollution to North America, Geophys. Res. Lett., 26, 711–714, 1999.
Kim, Y. P. and Seinfeld, J. H.: Atmospheric Gas-Aerosol Equilibrium. 3. Thermodynamics of Crustal Elements Ca2+, K+, and Mg2+, Aerosol Sci. Tech., 22, 93–110, 1995.
Kurata, G., Carmichael, G. R., Streets, D. G., Kitada, T., Tang, Y., Woo, J. H., and Thongboonchoo, N.: Relationships between emission sources and air mass characteristics in East Asia during the TRACE-P period, Atmos. Environ., 38, 6977–6987, 2004.

Lathière, J., Hauglustaine, D. A., Friend, A. D., De Noblet-Ducoudré, N., Viovy, N., and Folberth, G. A.: Impact of climate variability and land use changes on global biogenic volatile organic compound emissions, Atmos. Chem. Phys., 6, 2129–2146, 2006, http://www.atmos-chem-phys.net/6/2129/2006/.

Levy, H., Schwarzkopf, M. D., Horowitz, L., Ramaswamy, V., and Findell, K. L.: Strong sensitivity of late 21st century climate to projected changes in short-lived air pollutants, J. Geophys. Res.-Atmos., 113, D06102, doi:06110.01029/02007JD009176, 2008.

Liang, Q., Jaegle, L., Jaffe, D. A., Weiss-Penzias, P., Heckman, A., and Snow, J. A.: Long-range transport of Asian pollution to the northeast Pacific: Seasonal variations and transport pathways of carbon monoxide, J. Geophys. Res.-Atmos., 109, D23S07, doi:10.1029/2003JD004402, 2004.

Madronich, S.: The Tropospheric Visible Ultra-violet (TUV) model web page: http://www.acd.ucar.edu/TUV, 2002.

Mao, J., Ren, X., Brune, W. H., Olson, J. R., Crawford, J. H., Fried, A., Huey, L. G., Cohen, R. C., Heikes, B., Singh, H. B., Blake, D. R., Sachse, G. W., Diskin, G. S., Hall, S. R., and Shetter, R. E.: Airborne measurement of OH reactivity during INTEX-B, Atmos. Chem. Phys., 9, 163–173, 2009, http://www.atmos-chem-phys.net/9/163/2009/.

McNaughton, C. S., Clarke, A. D., Kapustin, V., Shinozuka, Y., Howell, S. G., Anderson, B. E., Winstead, E., Dibb, J., Scheuer, E., Cohen, R. C., Wooldridge, P., Perring, A., Huey, L. G., Kim, S., Jimenez, J. L., Dunlea, E. J., DeCarlo, P. F., Wennberg, P. O., Crounse, J. D., Weinheimer, A. J., and Flocke, F.: Observations of heterogeneous reactions between Asian pollution and mineral dust over the Eastern North Pacific during INTEX-B, Atmos. Chem. Phys. Discuss., 9, 8469–8539, 2009, http://www.atmos-chem-phys-discuss.net/9/8469/2009/.

Mena-Carrasco, M., Tang, Y., Carmichael, G. R., Chai, T., Thongbongchoo, N., Campbell, J. E., Kulkarni, S., Horowitz, L., Vukovich, J., Avery, M., Brune, W., Dibb, J. E., Emmons, L., Flocke, F., Sachse, G. W., Tan, D., Shetter, R., Talbot, R. W., Streets, D. G., Frost, G., and Blake, D.: Improving regional ozone modeling through systematic evaluation of errors using the aircraft observations during the International Consortium for Atmospheric Research on Transport and Transformation, J. Geophys. Res.-Atmos., 112, D12S19, doi:10.1029/2006JD007762, 2007.

Olivier, J. G. J. and Berdowski, J. J. M.: Global emissions sources and sinks, in: The Climate System, edited by: Guicherit, R. and Heij, B. J., A.A. Balkema Publishers/Swets & Zeitlinger Publishers, Lisse, The Netherlands, 33–78, 2001.

Pfister, G. G., Emmons, L. K., Hess, P. G., Lamarque, J. F., Orlando, J. J., Walters, S., Guenther, A., Palmer, P. I., and Lawrence, P. J.: Contribution of isoprene to chemical budgets: A model tracer study with the NCAR CTM MOZART-4, J. Geophys. Res.-Atmos., 113, D02204, doi:02210.01029/02007JD008797, 2008.

Reidmiller, D. R., Jaffe, D. A., Chand, D., Strode, S., Swartzendruber, P., Wolfe, G. M., and Thornton, J. A.: Interannual variability of long-range transport as seen at the Mt. Bachelor observatory, Atmos. Chem. Phys., 9, 557–572, 2009, http://www.atmos-chem-phys.net/9/557/2009/.

Seinfeld, J. H., Carmichael, G. R., Arimoto, R., Conant, W. C., Brechtel, F. J., Bates, T. S., Cahill, T. A., Clarke, A. D., Doherty, S. J., Flatau, P. J., Huebert, B. J., Kim, J., Markowicz, K. M., Quinn, P. K., Russell, L. M., Russell, P. B., Shimizu, A., Shinozuka, Y., Song, C. H., Tang, Y. H., Uno, I., Vogelmann, A. M., Weber, R. J., Woo, J. H., and Zhang, X. Y.: ACE-ASIA – Regional climatic and atmospheric chemical effects of Asian dust and pollution, B. Am. Meteorol. Soc., 85, 367–380, 2004.

Shinozuka, Y., Clarke, A. D., DeCarlo, P. F., Jimenez, J. L., Dunlea, E. J., Roberts, G. C., Tomlinson, J. M., Collins, D. R., Howell, S. G., Kapustin, V. N., McNaughton, C. S., and Zhou, J.: Aerosol optical properties relevant to regional remote sensing of CCN activity and links to their organic mass fraction: airborne observations over Central Mexico and the US West Coast during MILAGRO/INTEX-B, Atmos. Chem. Phys. Discuss., 9, 12519–12558, 2009, http://www.atmos-chem-phys-discuss.net/9/12519/2009/.

Singh, H. B., Brune, W. H., Crawford, J. H., Flocke, F., and Jacob, D. J.: Chemistry and transport of pollution over the Gulf of Mexico and the Pacific: spring 2006 INTEX-B campaign overview and first results, Atmos. Chem. Phys., 9, 2301–2318, 2009, http://www.atmos-chem-phys.net/9/2301/2009/.

Skamarock, W. C., Klemp, J. B., Dudhia, J., Gill, D. O., Barker, D. M., Wang, W., and Powers, J. G.: A description of the Advanced Research WRF Version 2, NCAR Tech Notes-468+STR, 2005.

Streets, D. G., Bond, T. C., Carmichael, G. R., Fernandes, S. D., Fu, Q., He, D., Klimont, Z., Nelson, S. M., Tsai, N. Y., Wang, M. Q., Woo, J. H., and Yarber, K. F.: An inventory of gaseous and primary aerosol emissions in Asia in the year 2000, J. Geophys. Res.-Atmos., 108, 8809, doi:8810.1029/2002JD003093, 2003.

Tang, Y. H., Carmichael, G. R., Uno, I., Woo, J. H., Kurata, G., Lefer, B., Shetter, R. E., Huang, H., Anderson, B. E., Avery, M. A., Clarke, A. D., and Blake, D. R.: Impacts of

aerosols and clouds on photolysis frequencies and photochemistry during TRACE-P: 2. Three-dimensional study using a regional chemical transport model, J. Geophys. Res.-Atmos., 108, 8822, doi:8810.1029/2002JD003100, 2003.

Tang, Y., Carmichael, G. R., Horowitz, L. W., Uno, I., Woo, J.-H., Streets, D. G., Dabdub, D., Kurata, G., Sandu, A., Allan, J., Atlas, E., Flocke, F., Huey, L. G., Jakoubek, R. O., Millet, D. B., Quinn, P. K., Roberts, J. M., Worsnop, D. R., Goldstein, A., Donnelly, S., Schauffler, S., Stroud, V., Johnson, K., Avery, M. A., Singh, H. B., and Apel, E. C.: Multiscale simulations of tropospheric chemistry in the eastern Pacific and on the US West Coast during spring 2002, J. Geophys. Res., 109, D23S11, doi:10.1029/2004JD004513, 2004a.

Tang, Y. H., Carmichael, G. R., Kurata, G., Uno, I., Weber, R. J., Song, C. H., Guttikunda, S. K., Woo, J. H., Streets, D. G., Wei, C., Clarke, A. D., Huebert, B., and Anderson, T. L.: Impacts of dust on regional tropospheric chemistry during the ACE-Asia experiment: A model study with observations, J. Geophys. Res.-Atmos., 109, D19S21, doi:10.1029/2003JD003806, 2004b.

Tang, Y. H., Carmichael, G. R., Thongboonchoo, N., Chai, T. F., Horowitz, L. W., Pierce, R. B., Al-Saadi, J. A., Pfister, G., Vukovich, J. M., Avery, M. A., Sachse, G. W., Ryerson, T. B., Holloway, J. S., Atlas, E. L., Flocke, F. M., Weber, R. J., Huey, L. G., Dibb, J. E., Streets, D. G., and Brune, W. H.: Influence of lateral and top boundary conditions on regional air quality prediction: A multiscale study coupling regional and global chemical transport models, J. Geophys. Res.-Atmos., 112, D10S18, doi:10.1029/2006JD007515, 2007.

Turpin, B. J. and Lim, H. J.: Species contributions to $PM_{2.5}$ mass concentrations: Revisiting common assumptions for estimating organic mass, Aerosol Sci. Tech., 35(1), 602–610, 2001.

Uno, I., Satake, S., Carmichael, G. R., Tang, Y. H., Wang, Z. F., Takemura, T., Sugimoto, N., Shimizu, A., Murayama, T., Cahill, T. A., Cliff, S., Uematsu, M., Ohta, S., Quinn, P. K., and Bates, T. S.: Numerical study of Asian dust transport during the springtime of 2001 simulated with the Chemical Weather Forecasting System (CFORS) model, J. Geophys. Res.-Atmos., 109, D19S24, doi:10.1029/2003JD004222, 2004.

VanCuren, R. A.: Asian aerosols in North America: Extracting the chemical composition and mass concentration of the Asian continental aerosol plume from long-term aerosol records in the western United States, J. Geophys. Res.-Atmos., 108, 4623, doi:4610.1029/2003JD003459, 2003.

van Donkelaar, A., Martin, R. V., Leaitch, W. R., Macdonald, A. M., Walker, T. W., Streets, D. G., Zhang, Q., Dunlea, E. J., Jimenez, J. L., Dibb, J. E., Huey, L. G., Weber, R., and

Andreae, M. O.: Analysis of aircraft and satellite measurements from the Intercontinental Chemical Transport Experiment (INTEX-B) to quantify long-range transport of East Asian sulfur to Canada, Atmos. Chem. Phys., 8, 2999–3014, 2008, http://www.atmos-chem-phys.net/8/2999/2008/.

Volkamer, R., Jimenez, J. L., San Martini, F., Dzepina, K., Zhang, Q., Salcedo, D., Molina, L. T., Worsnop, D. R., and Molina, M. J.: Secondary Organic Aerosol Formation from Anthropogenic Air Pollution: Rapid and Higher than Expected, Geophys. Res. Lett., 33, L17811, doi:17810.11029/12006GL026899, 2006.

Wolfe, G. M., Thornton, J. A., McNeill, V. F., Jaffe, D. A., Reidmiller, D., Chand, D., Smith, J., Swartzendruber, P., Flocke, F., and Zheng, W.: Influence of trans-Pacific pollution transport on acyl peroxy nitrate abundances and speciation at Mount Bachelor Observatory during INTEX-B, Atmos. Chem. Phys., 7, 5309–5325, 2007, http://www.atmos-chem-phys.net/7/5309/2007/.

Yienger, J. J., Galanter, M., Holloway, T. A., Phadnis, M. J., Guttikunda, S. K., Carmichael, G. R., Moxim, W. J., and Levy, H.: The episodic nature of air pollution transport from Asia to North America, J. Geophys. Res.-Atmos., 105, 26931–26945, 2000.

Zhang, L., Jacob, D. J., Boersma, K. F., Jaffe, D. A., Olson, J. R., Bowman, K. W., Worden, J. R., Thompson, A. M., Avery, M. A., Cohen, R. C., Dibb, J. E., Flock, F. M., Fuelberg, H. E., Huey, L. G., McMillan, W. W., Singh, H. B., and Weinheimer, A. J.: Transpacific transport of ozone pollution and the effect of recent Asian emission increases on air quality in North America: an integrated analysis using satellite, aircraft, ozonesonde, and surface observations, Atmos. Chem. Phys., 8, 6117–6136, 2008, http://www.atmos-chem-phys.net/8/6117/2008/.

Zhang, Q., Streets, D. G., Carmichael, G. R., He, K. B., Huo, H., Kannari, A., Klimont, Z., Park, I. S., Reddy, S., Fu, J. S., Chen, D., Duan, L., Lei, Y., Wang, L. T., and Yao, Z. L.: Asian emissions in 2006 for the NASA INTEX-B mission, Atmos. Chem. Phys., 9, 5131–5153, 2009, http://www.atmos-chem-phys.net/9/5131/2009/.

Zhang, Q., Jimenez, J. L., Canagaratna, M. R., et al.: Ubiquity and Dominance of Oxygenated Species in Organic Aerosols in Anthropogenically-Influenced Northern Hemisphere Midlatitudes, Geophys. Res. Lett., 34, L13801, doi:10.1029/2007GL029979, 2007.

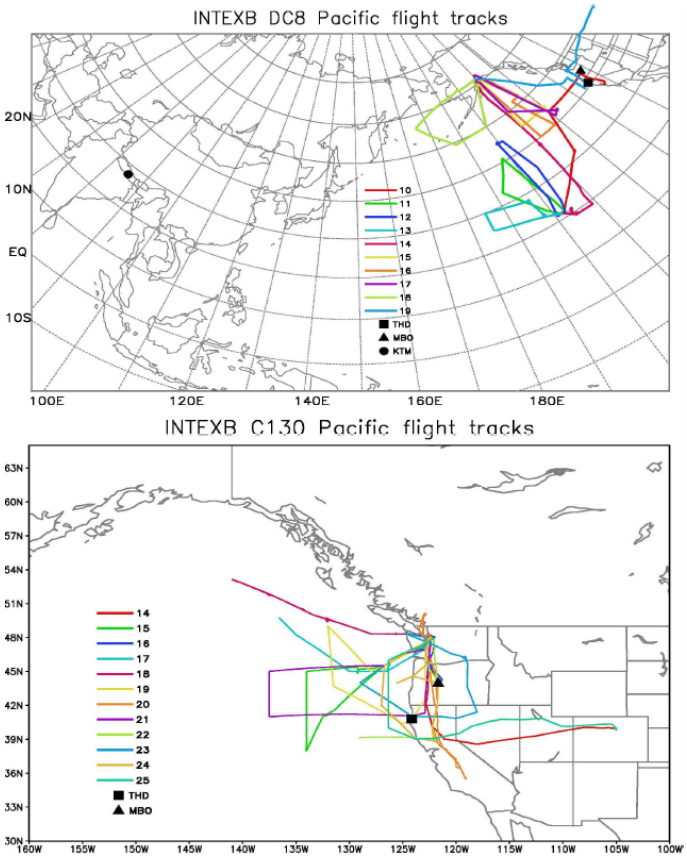

Fig. 1. NASA DC-8 and NCAR/NSF C-130 flight tracks along with the location of ground based observation sites including Kathmandu (KTM), Trinidad Head (THD) and Mt. Bachelor (MBO) during the INTEX-B (Phase 2) experiment. The numbers denote the research flight numbers for the DC-8 and C-130 aircraft.

ACPD
9, 16381–16439, 2009

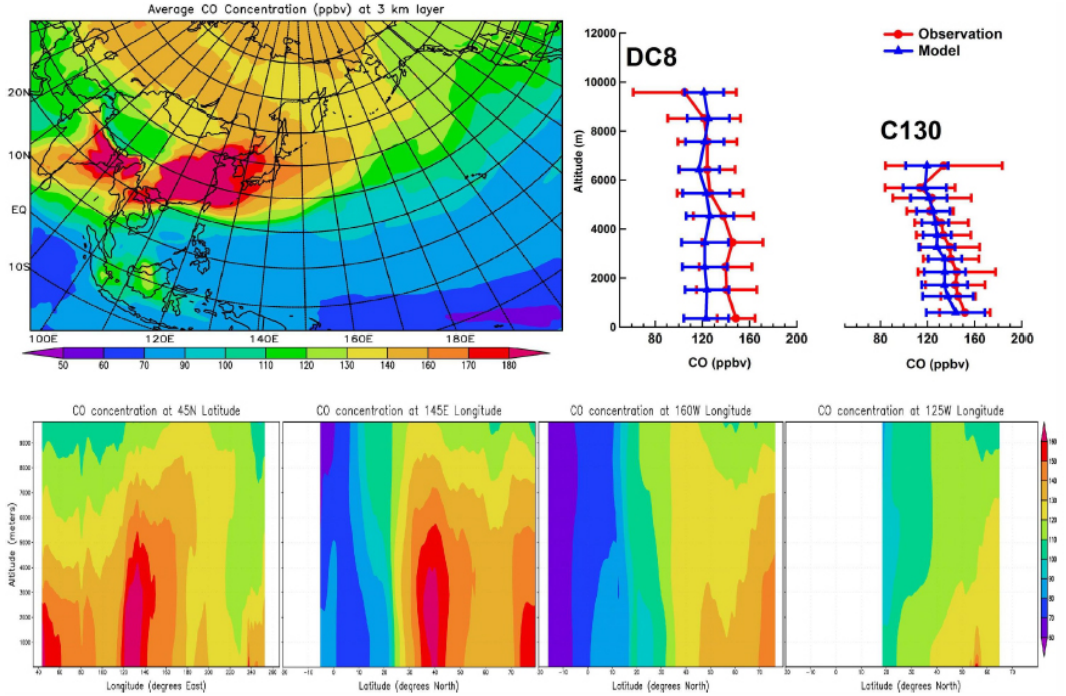

Fig. 2. (a) Mission wide average CO at 3 km AGL layer (b) DC-8 and C-130 observed and modeled CO vertical profiles (c) Average CO latitudinal and longitudinal distributions during INTEX-B study period.

ACPD
9, 16381–16439, 2009

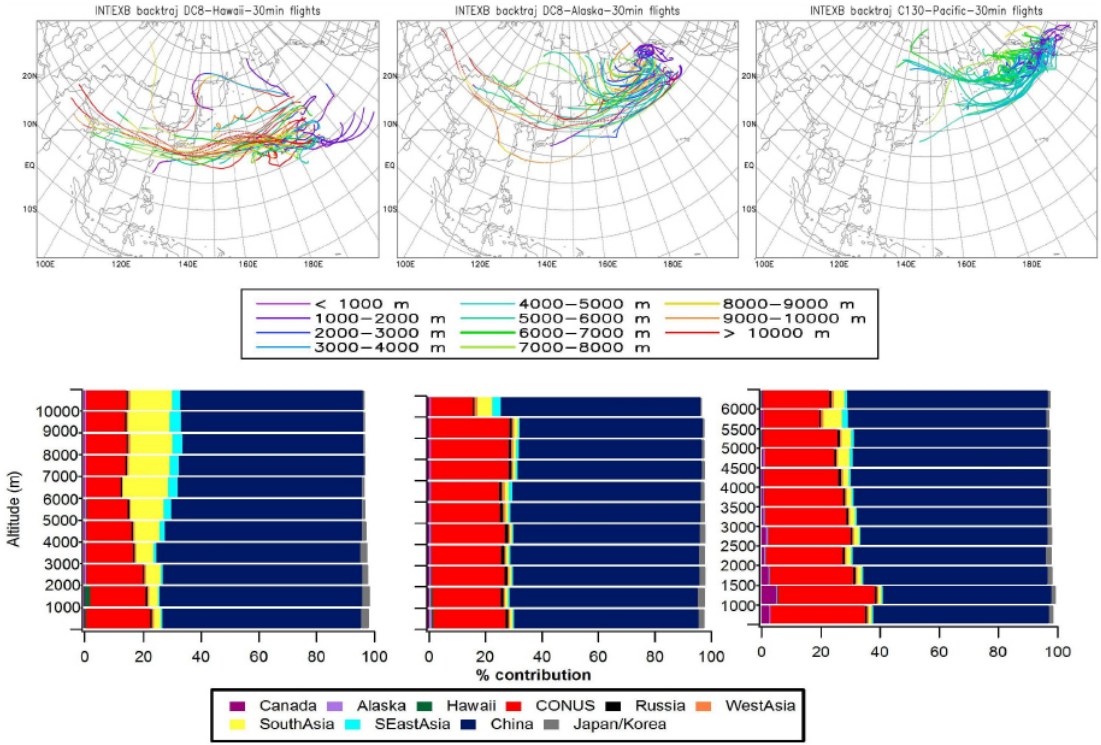

Fig. 3. Back trajectories of wind vectors and tagged anthropogenic CO tracers illustrating the source region of air masses sampled by the selected DC-8 and C-130 flights.

ACPD
9, 16381–16439, 2009

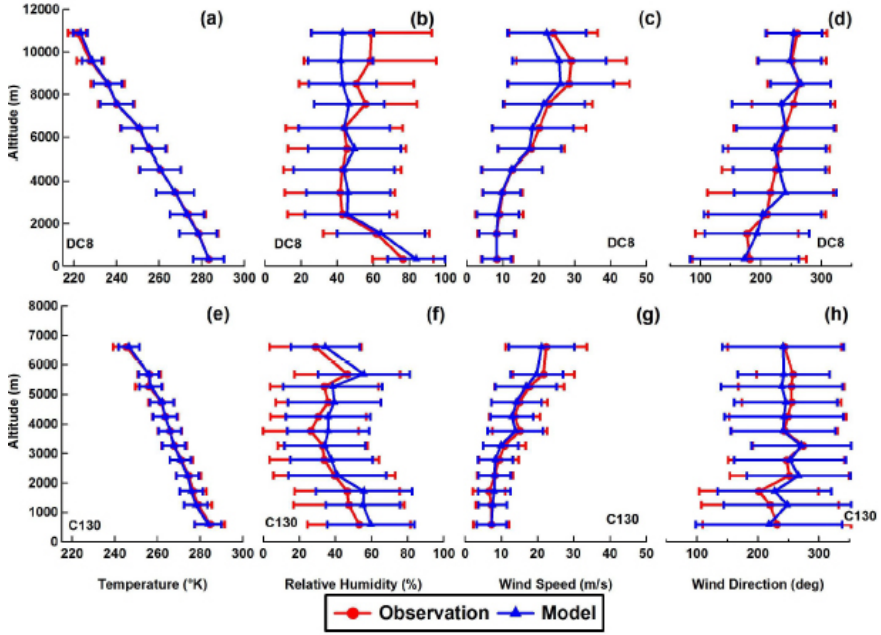

Fig. 4. Comparison of meteorological variables from the WRF model with DC-8 (Top row **a**, **b**, **c**, **d**) and C-130 (bottom row **e**, **f**, **g**, **h**) observations.

ACPD
9, 16381–16439, 2009

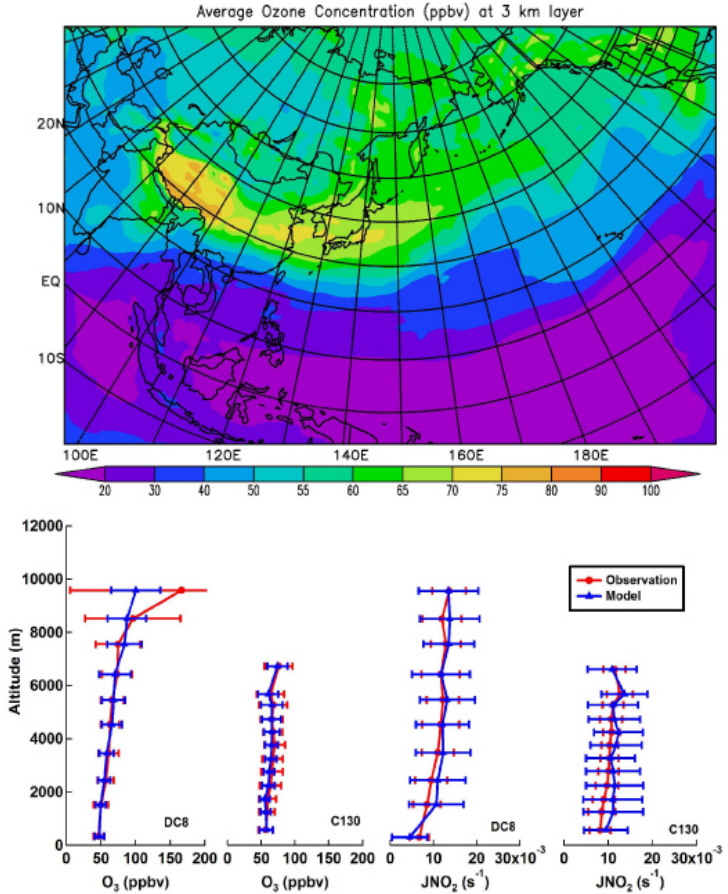

Fig. 5. Mission wide average ozone at 3 km AGL layer along with DC-8 and C-130 observed and modeled vertical profiles of ozone and photolysis rate of NO_2 (JNO_2).

ACPD

9, 16381–16439, 2009

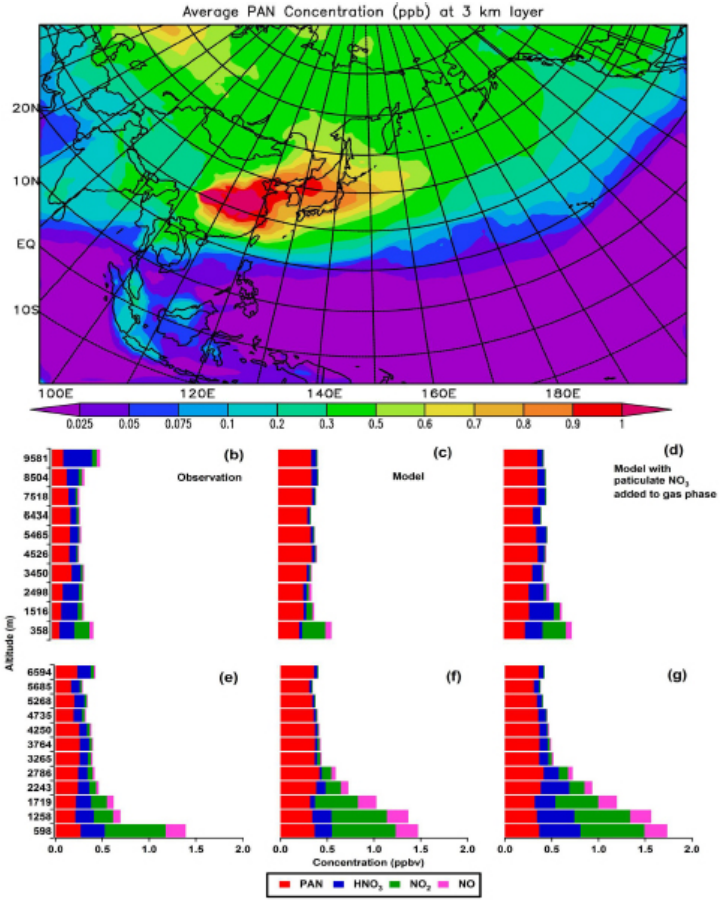

Fig. 6. Mission wide average PAN at 3 km AGL layer **(a)** along with comparison of model predicted and observed NO_y components of DC-8 **(b, c, d)** and C-130 **(e, f, g)**.

ACPD
9, 16381–16439, 2009

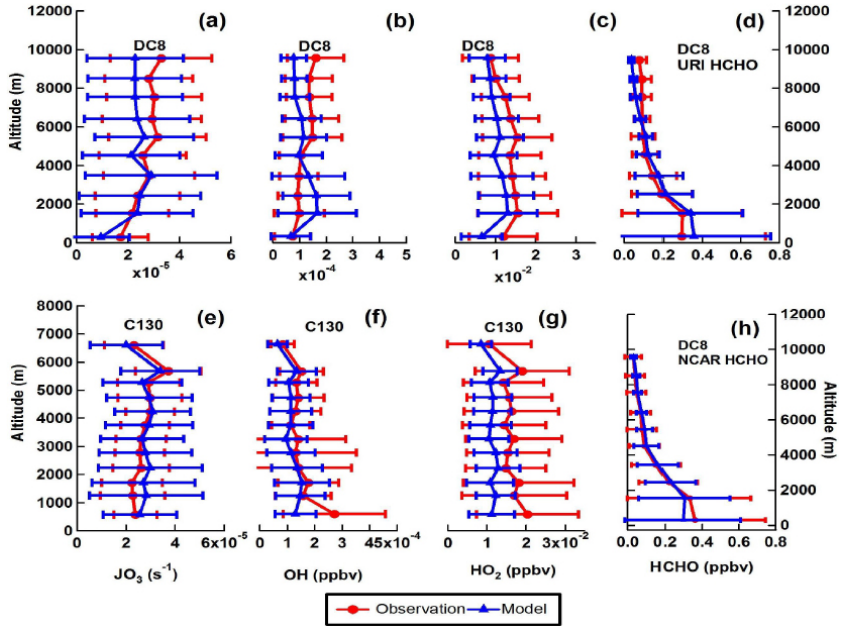

Fig. 7. Comparison of STEM model predictions with DC-8 and C-130 observations of ozone photolysis rate (JO_3), HO_x (OH and HO_2) species and Formaldehyde (HCHO).

ACPD
9, 16381–16439, 2009

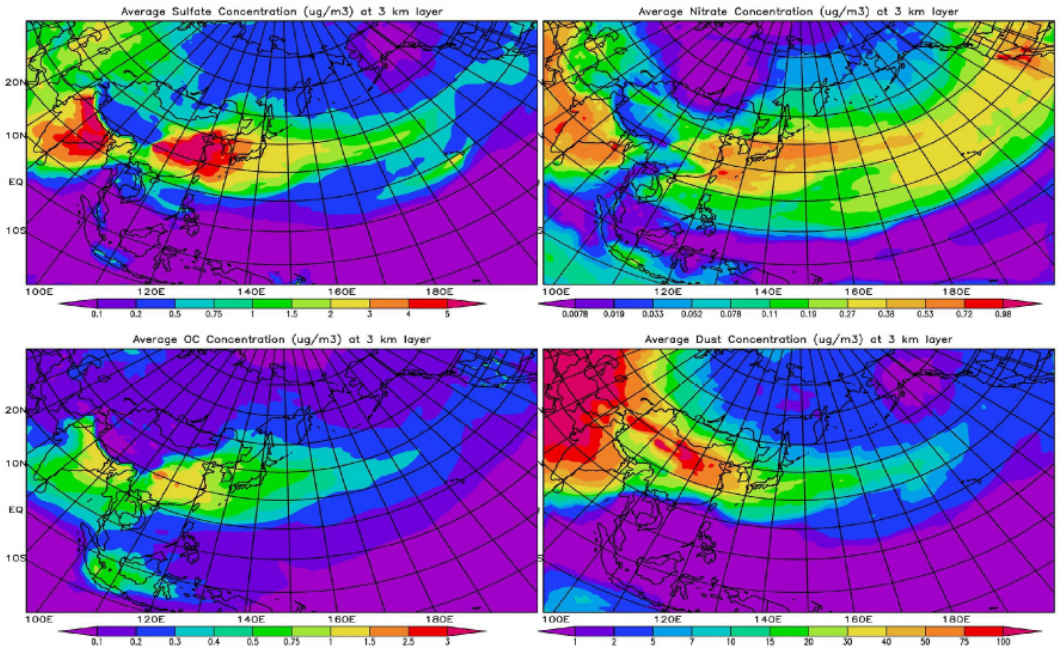

Fig. 8. Mission wide average distribution of aerosols at the 3-km AGL layer (a) Sulfate, (b) Nitrate, (c) OC and (d) Dust during INTEX-B.

ACPD
9, 16381–16439, 2009

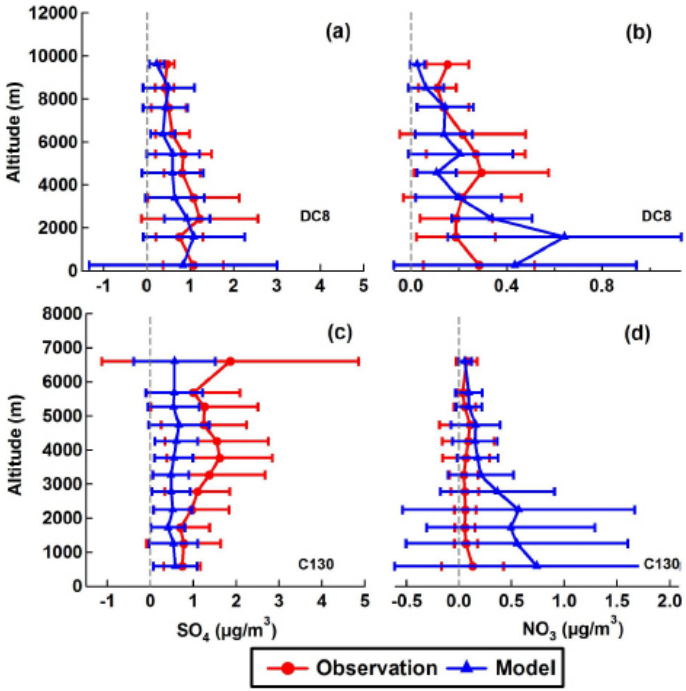

Fig. 9. Comparison of STEM model predictions versus observed aerosols from the DC-8 and C-130 **(a)** Sulfate (DC-8) **(b)** NO_3 (DC-8) **(c)** Sulfate (C-130) and **(d)** NO_3 (C-130).

ACPD
9, 16381–16439, 2009

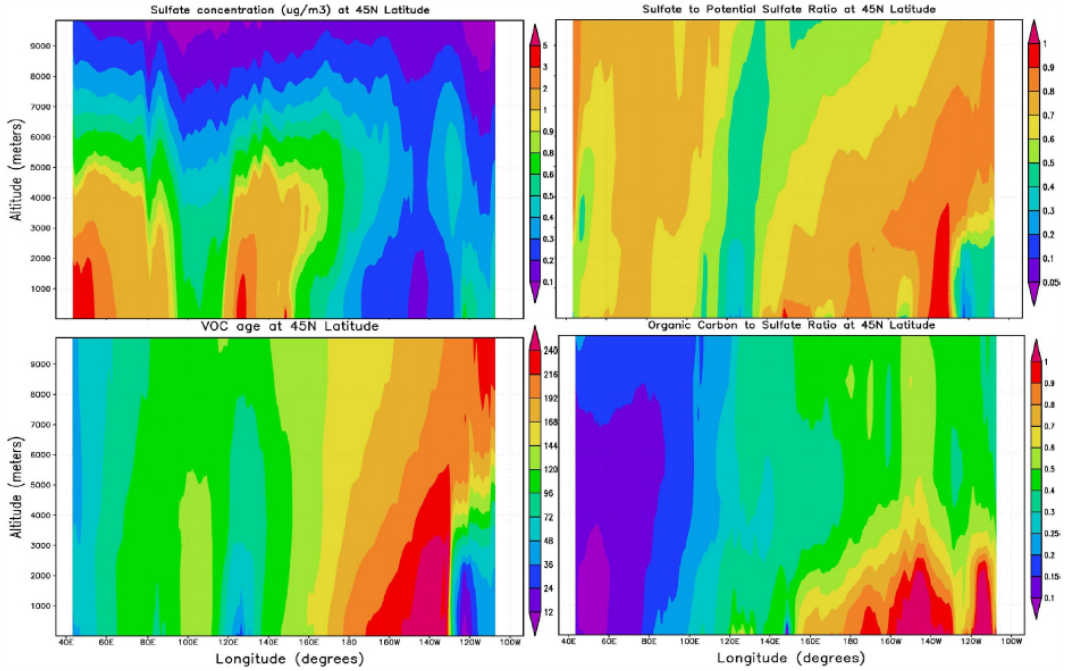

Fig. 10. Mission wide average cross-sections of (a) sulfate (b) sulfate to potential sulfate ratio (c) VOC age (hours) and (d) OC/SO_4 ratio at 45 N during INTEX-B.

ACPD
9, 16381–16439, 2009

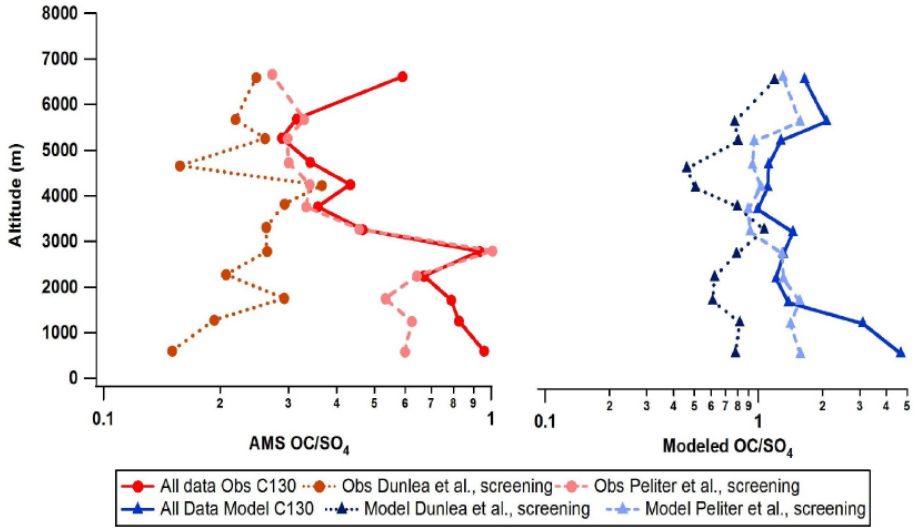

Fig. 11. Average vertical profiles of OC/SO_4 ratio for INTEX-B campaign. The observed OC/SO_4 ratio is calculated using the OC (OM/1.9) and SO_4 measurements from AMS aboard the C-130 aircraft. The Dunlea et al. (2008) screening criteria are Observed AMS $SO_4 > 1\ \mu g/m^3$ and sampled west of 125 W degrees longitude. The Peltier et al. (2008) criteria used are modeled CO>100 ppb and model tagged China anthropogenic CO>50% of the predicted total anthropogenic CO.

ACPD
9, 16381–16439, 2009

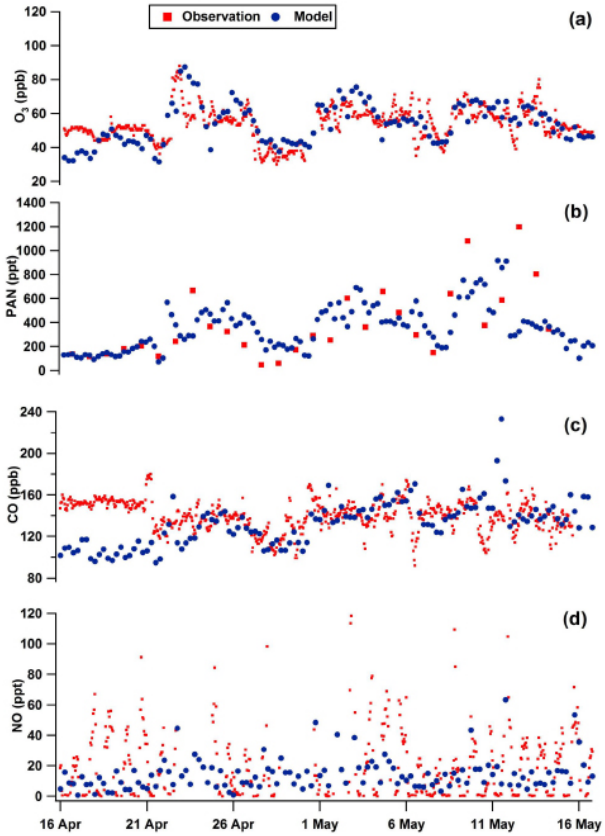

Fig. 12. Comparison of observed and modeled trace gases at Mt. Bachelor (MBO), OR during INTEX-B campaign **(a)** Ozone **(b)** PAN **(c)** CO **(d)** NO.

ACPD
9, 16381–16439, 2009

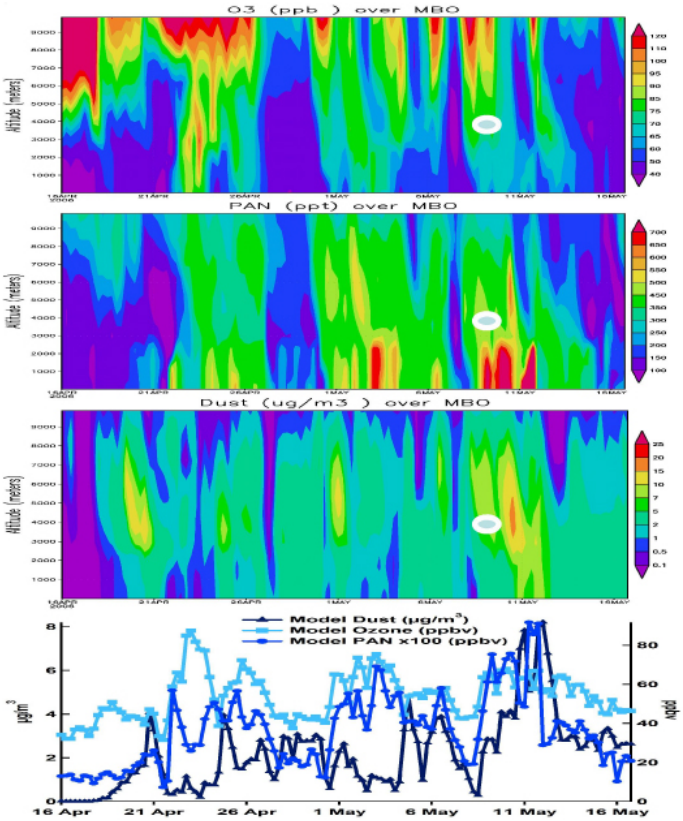

Fig. 13. Curtain plots of modeled trace gases at Mt. Bachelor (MBO), OR during INTEX-B campaign (a) Ozone (b), PAN, (c) Dust along with (d) time series of these species at the surface level. The white oval shape denotes the lagrangian air mass sampled by C130 flight 21 (5 May 2006) that arrived at MBO on 8 May 2006.

ACPD
9, 16381–16439, 2009

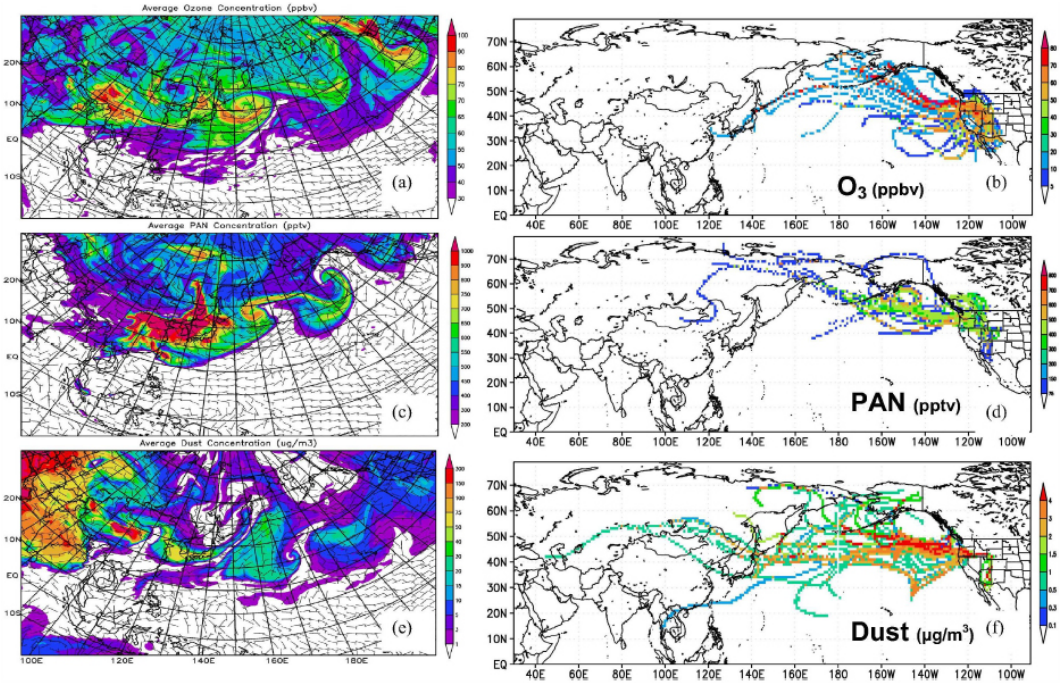

Fig. 14. Horizontal distribution of modeled ozone, PAN, and dust at 18 z, 3 km AGL layer along with redistributed concentration along back trajectories on 22 April **(a, b)**, 3 May **(c, d)** and 11 May **(e, f)** during INTEX-B.

ACPD
9, 16381–16439, 2009

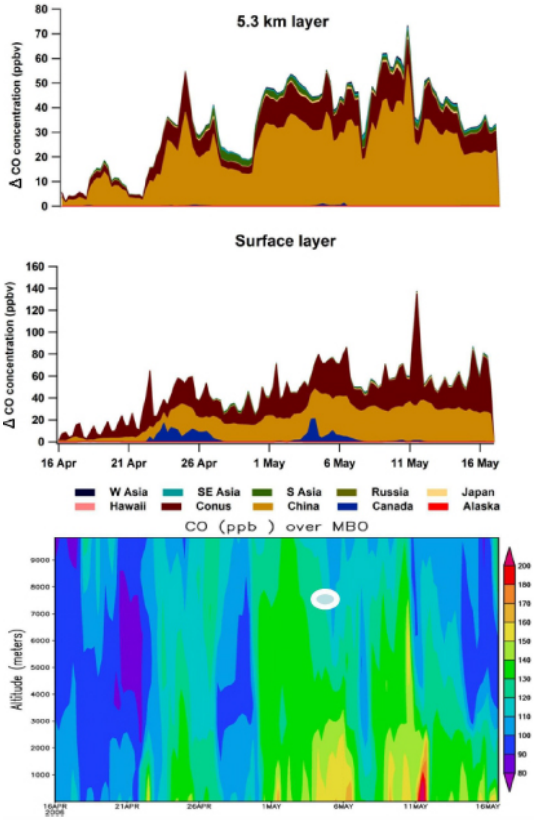

Fig. 15. Time series of source region tagged CO tracers at 5.3 km AGL layer (a) and surface (b) along with the vertical profile of CO (c) at Mt. Bachelor (MBO). The white oval denotes the location of the lagrangian sampled air mass sampled by C130 flight 21 (5 May 2006) that arrived at MBO on 8 May 2006.

ACPD
9, 16381–16439, 2009

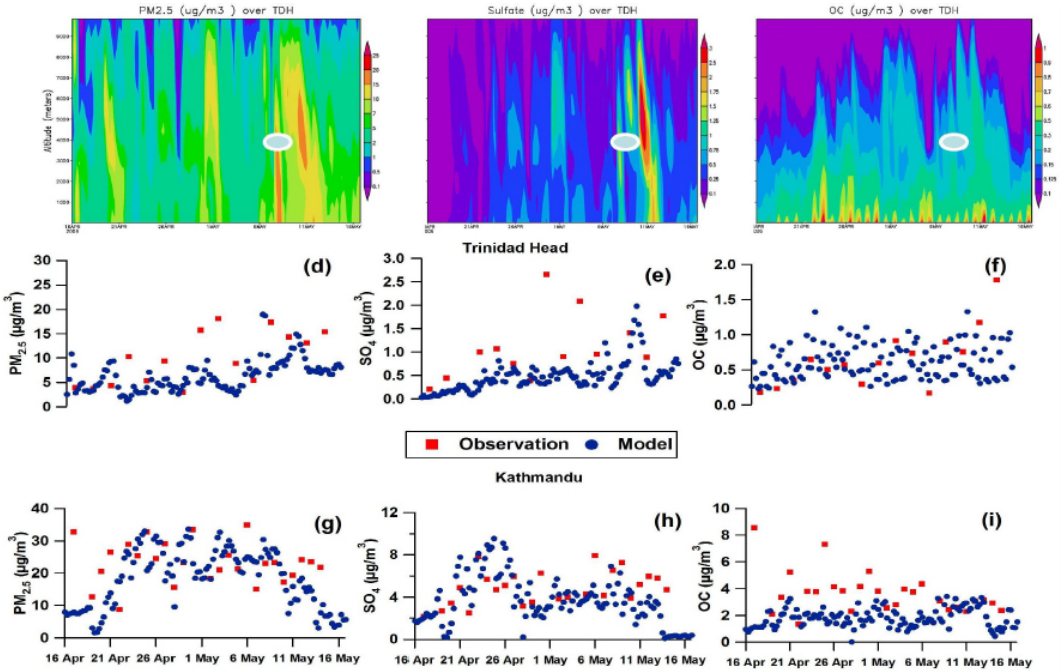

Fig. 16. Comparison of observed $PM_{2.5}$, sulfate and OC at Trinidad Head (THD), US (middle row) and Kathmandu, Nepal (bottom) during the INTEX-B campaign Top row curtain plots at THD. The white oval denotes the location of the lagrangian sampled air mass sampled by C130 flight 21 (5 May 2006) that arrived at THD on 8 May 2006.

ACPD
9, 16381–16439, 2009

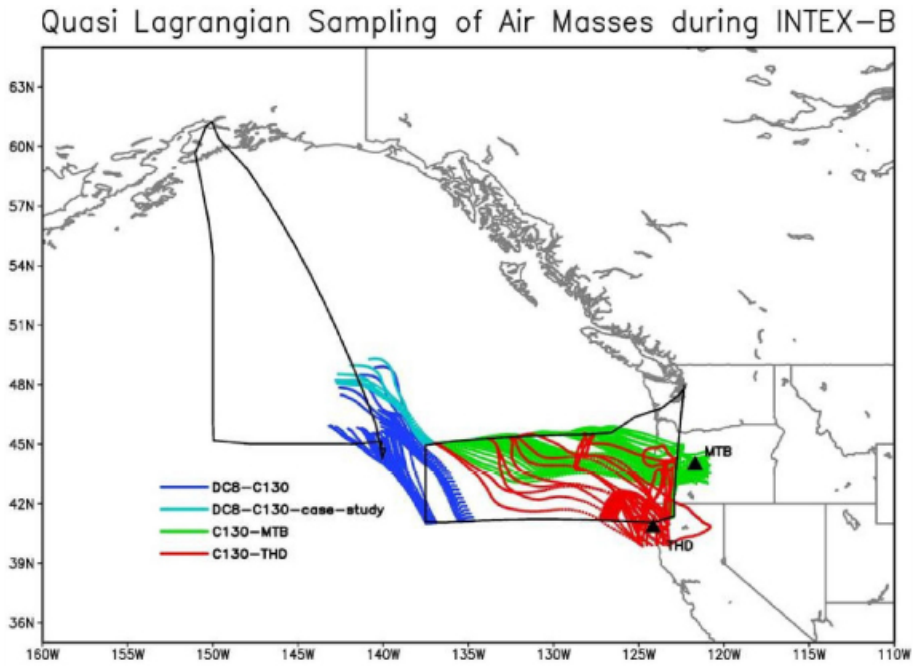

Fig. 17. Quasi lagrangian sampling of air masses between DC-8 flight 15 (4 May 2006), C-130 flight 21 (5 May 2006), and the two surface sites Mt. Bachelor (MBO) (8 May 2006) and Trinidad Head (THD) (8 May 2006) during INTEX-B.

ACPD
9, 16381–16439, 2009

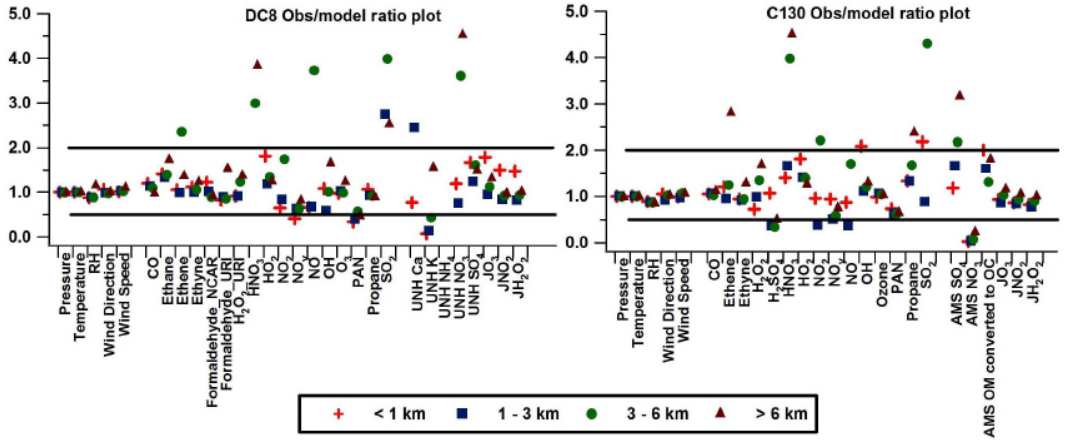

Fig. 18. Ratio of observed to model predicted mean values of (a) DC-8 and (b) C-130 airborne measurements.

ACPD
9, 16381–16439, 2009

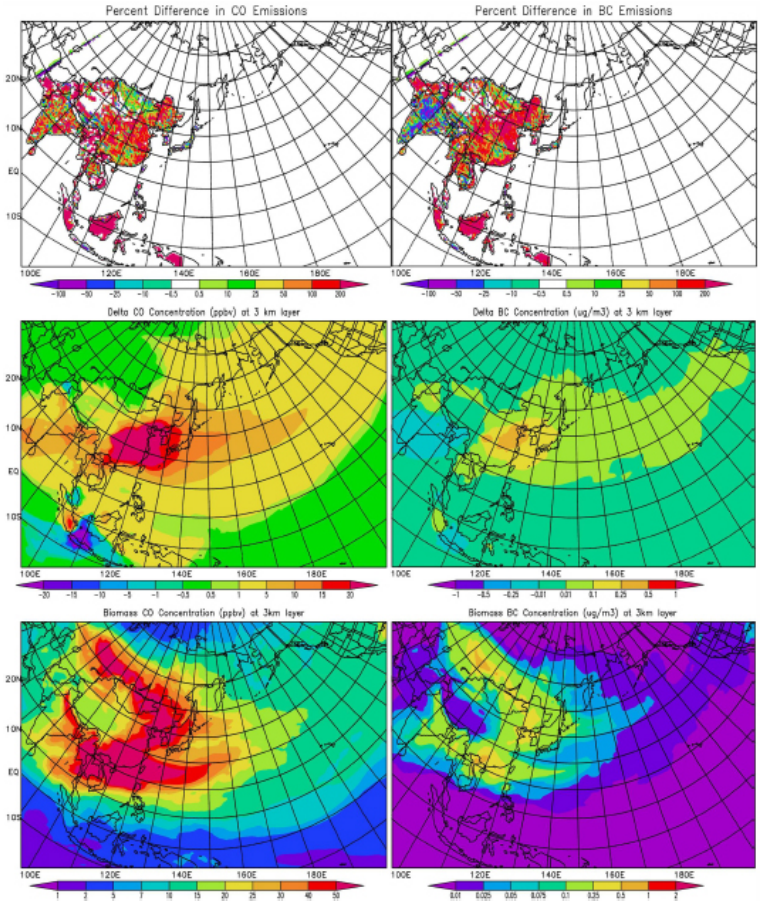

Fig. 19. Changing Asian emissions from 2000 to 2006 and its impact on concentration at the 3 km AGL layer during INTEX-B.

ACPD

9, 16381–16439, 2009

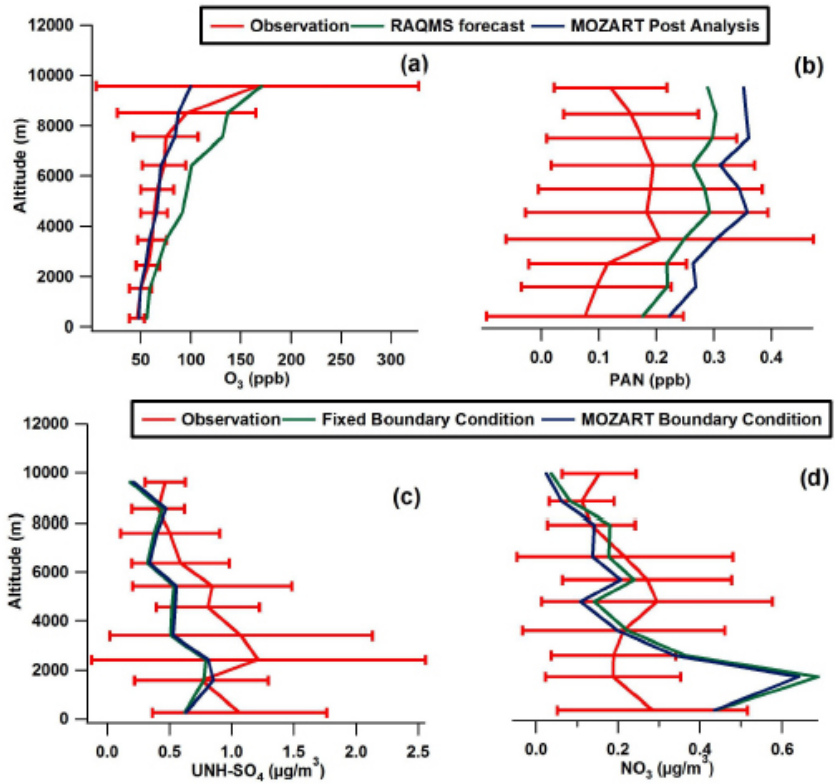

Fig. 20. Influence of global model and fixed boundary condition on trace gases and aerosols during INTEX-B.

ACPD
9, 16381–16439, 2009

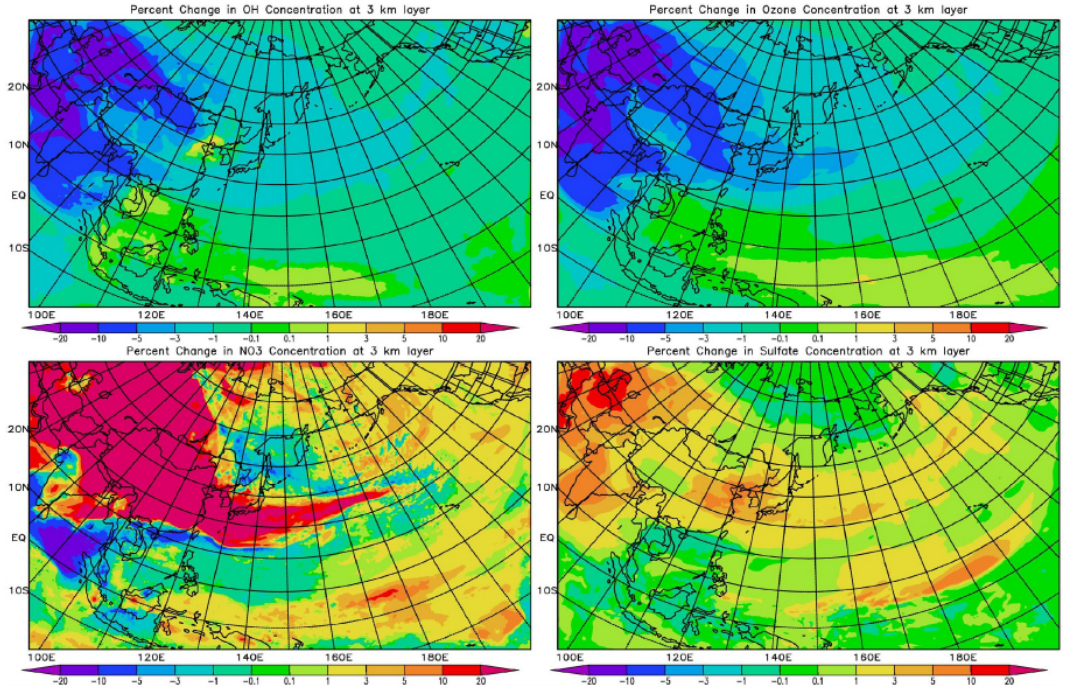

Fig. 21. Two week averaged percent change in the conc. of OH, O_3, nitrate and sulfate without heterogeneous chem. during the Hawaii portion of INTEX-B mission. Shown are ((heterogeneous-without heterogeneous)/without heterogeneous)*100.

ACPD
9, 16381–16439, 2009

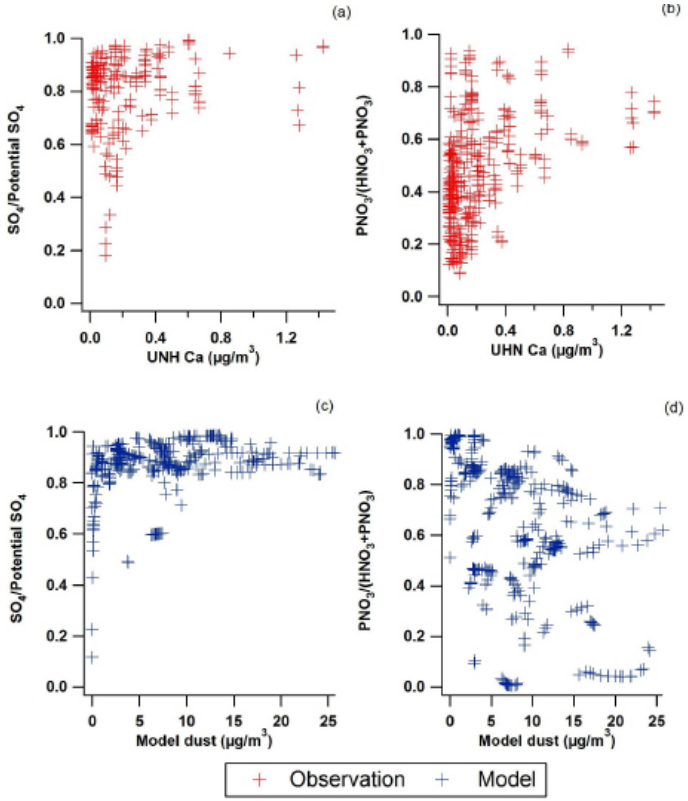

Fig. 22. Comparison of stem model predicted ratios with DC-8 observations **(a)** observed SO_4/Potential SO_4 ratio **(b)** observed aerosol NO_3/(aerosol NO_3 + HNO_3) **(c)** Modeled SO_4/Potential SO_4 ratio **(d)** Modeled aerosol NO_3/(aerosol NO_3 + HNO_3).

ACPD
9, 16381–16439, 2009

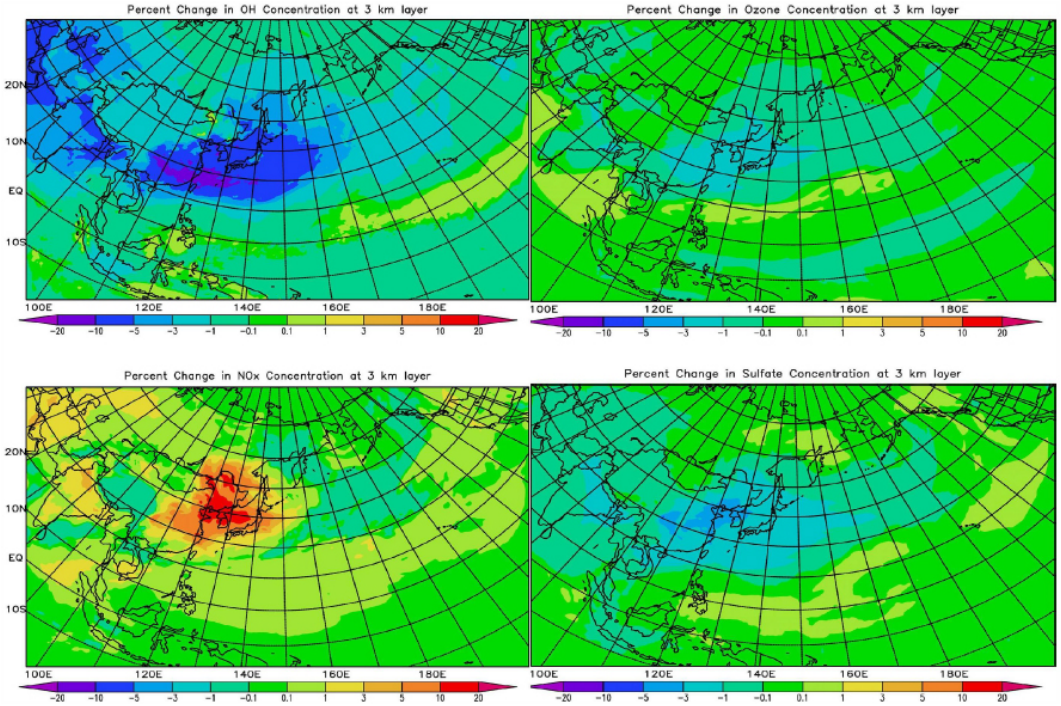

Fig. 23. Two week averaged percent change in the conc. of OH and O_3 without the contribution of aerosols in photolysis rate calculation during the Hawaii portion of INTEX-B. Shown are ((with aerosol-without aerosol)/without aerosol)*100.

ACPD
9, 16381–16439, 2009